Preprints (www.preprints.org) | NOT PEER-REVIEWED | Posted: 27 May 2021 doi:10.20944/preprints202105.0683.v1

Systematic Review of Centrifugal Valving Based on Digital Twin Modelling towards Highly Integrated Lab-on-a-Disc Systems

Jens Ducrée, School of Physical Sciences, Dublin City University, Ireland

Abstract

Current, application-driven trends towards larger-scale integration (LSI) of microfluidic systems for comprehensive assay automation and multiplexing pose significant technological and economical challenges. By virtue of their intrinsic capability for powerful sample preparation, centrifugal systems have attracted significant interest in academia and business since the early 1990s. This review models common, rotationally controlled valving schemes at the heart of "Lab-on-a-Disc" (LoaD) platforms to predict critical spin rates and reliability of flow control based on geometries, location and liquid volumes to be processed, and their experimental tolerances. The method presented here greatly facilitates simulation tools for virtual prototyping and characterization to greatly expedite design optimization according to key performance indicators (KPIs). This digital twin approach thus significantly accelerates, de-risks and lowers costs along the critical advancement from idea, fluidic testing, bioanalytical validation and scale-up to commercial mass manufacture.

Introduction

Since their inception in the early 1990s, an important design goal of microfluidic Lab-on-a-Chip or micro Total Analysis Systems (µTAS) [1] has been to "cram more components onto integrated circuits", and thus more functionality, onto a given piece of (chip) real estate. This objective is somewhat on the analogy of Moore's law [2] guiding miniaturization of microelectronics. Reducing structural dimensions is reasoned by technical aspects, e.g., functional integration for enabling modern, high-performance computers, smartphones and gadgets, and economic aspects as the cost of material and (typically pattern-transfer based) manufacturing processes strongly scales with the surface area of the chip [3]. "Price per functional unit", and thus the packing density, may hence be deemed the main driver of technology development.

While the general wish lists for cost and capabilities are quite alike, microfluidics-enabled (bio-)analytical technologies can often not be shrunk towards the nanoscale, for instance, to still guarantee the presence of a minimum number of analyte molecules or particles in the (bio-)sample for guaranteeing sufficient statistics, for meeting limits of detection, or due to drastic changes in dominant fluidic effects, such adverse surface interactions and evaporation, along increasing surface-to-volume ratios towards miniaturisation.

Over the recent decades, numerous "Lab-on-a-Chip" platforms have been developed, many of them conceived for decentralised biochemical testing. On the one hand, these microfluidic systems may enhance the analytical performance, e.g., through expediting the completion of transport processes, such driving diffusive mixing and heat exchange for short time-to-result, by imposing highly controlled conditions under strict laminarity at low Reynolds numbers, or by scale-matching with the bio-entities such as cells. On the other hand, miniaturization resides at the backbone of sample-to-

 doi:10.20944/preprints202105.0683.v1

answer automation and parallelization, e.g., as a crucial product requirement for deployment of bioassay panels at the point-of-use / point-of-care (PoC).

Lab-on-a-Chip systems frequently feature a modular setup where a microfluidic chip is inserted into a compact, rugged and potentially portable instrument equipped with a control unit, sensors, actuators and a pumping mechanism to process the liquid sample and reagents. The underlying, typically multi-branched channel architecture can usually not be properly washed to assure full regeneration of fluidic functionality, and also to avoid cross-contamination or carry-over of biosamples and reagents. Hence, in most cases, the chip has to be devised as single-use. The cost of material, equipment, process development and machine time of this disposable, which is normally mass-produced by tool-based polymer replication schemes such as injection moulding, increases with the volume of bulk material and the surface area; in addition, cost of postprocessing, e.g., coatings, barrier materials and reagents, as well as assembly steps, e.g., alignment of a lid, might be significant, thus possibly putting a commercially prohibitive price tag on disc real estate.

Amongst various Lab-on-a-Chip technologies addressing comprehensive process integration of bioanalytical protocols, we investigate here liquid handling by centrifugal microfluidics that has been successfully advanced in industry and academia since the mid-1990s [4-16] for various applications, mostly in the context of biomedical *in vitro* diagnostics (IVD) for deployment at the point-of-care (PoC). Other applications comprise liquid handling automation for the life sciences, e.g., concentration / purification and amplification of DNA / RNA from a range of biosamples, process analytical techniques and cell line development for biopharma as well as monitoring the environment, infrastructure, industrial processes and agrifood.

In such “Lab-on-a-Disc” (LoaD) systems, biochemical assays are ported on the rotationally controlled scheme by dissecting the often conventional, possibly volume-reduced protocol into a sequence of Laboratory Unit Operation (LUOs) such as metering / aliquoting [17-19], mixing [20-23], incubation, purification / concentration / extraction [24, 25], homogenisation [26, 27], particle filtering [28-32] and droplet generation [33-35]. These LUOs are mostly processed in a batch-wise, rather than a continuous fashion, by transiently sealing their fluidic exit with a normally-closed valve, thus intermittently stopping the flow while continuing rotation within certain boundaries, e.g., for rotationally induced agitation of the liquid sample.

These centrifugal LUOs and their linked downstream detection techniques have been comprehensive reviewed elsewhere [14-16, 36-42]. The various centrifugal platforms predominantly distinguish by their valving mechanism, which critically determines their capability for functional multiplexing [43]. Most of these flow control schemes root in the interplay of the centrifugal pressure exerted on a rotor-based liquid volume with a counteracting effect. Initial concepts were mainly based on interfacial tension to create capillary burst valves or siphons primed by capillary action which open by lifting [10], lowering [5] or accelerating [44] the spin rate across critical thresholds.

Furthermore, active pneumatic pumping by external or onboard pressure sources [25, 43, 45], by thermo-pneumatic actuation [19] and chemical reactions [46] have been demonstrated. Yet, at least as stand-alone, such active concepts tend to be hard to fine control or stabilise over the lifetime of the chip, ranging from production, packaging, storage and transport to eventual handling by the user and processing on a PoC instrument; they also lack to provide a physical vapour barrier, hence making them unsuitable for longer-term onboard storage of liquid reagents as an important feature for many PoC scenarios.

Preprints (www.preprints.org) | NOT PEER-REVIEWED | Posted: 27 May 2021 doi:10.20944/preprints202105.0683.v1

To this end, several normally-closed valving schemes employing sacrificial barriers for retention of liquids and their vapour were introduced. In most implementations, the barrier is opened by an instrument- or rotor-based power unit [47], e.g., for mechanical [48], laser- [49-54] or heat-induced perforation of a film [55], melting of a wax plug [56] or magnetic deflection of membranes during rotation or at rest. Also, passive, solvent-selective barriers have been explored [32, 47, 57], which only transmit flow upon distinct physico-chemical stimuli.

More recently, centrifugo-pneumatic (CP) siphon valves were developed [18, 44, 58-60] where air is entrapped and centrifugally compressed by the incoming liquid during filling in a side chamber. Upon lowering the spin rate ω, the expansion of the pressurised volume pushes a surface-tension stabilized liquid "piston" across the crest point of the outlet siphon. This "Lab-on-a-Disc" (LoaD) platform uses a gas-impermeable, dissolvable film (DF) which is initially protected by a neighbouring gas pocket. Once a geometry-dependent critical spin rate Ω is surpassed, the forward meniscus wets the DF to thus, at the same time, vent the compression chamber and open a downstream outlet. Based on this conceptually simple CP-DF scheme [61, 62], which can be solely controlled by the system-innate spindle motor, the integration of LoaD systems has been considerably elevated [57, 61-63].

This work will significantly advance this work by providing a general "digital twin" methodology for optimising fluidic performance, robustness, packing density and manufacturability of rotationally controlled valving schemes for LoaD platforms. The first section surveys the fundamentals of centrifugal fields, continuity of mass and pressures contributing to hydrostatic equilibria at the core of valving liquid samples and reagents during batch-wise processing of their upstream LUOs. We then elaborate the concepts of critical spin rates and their associated band widths as quantitative, key performance indicators (KPIs) for systematically assessing the impact of experimental and geometrical tolerances on operational reliability at component- and system-level.

The next section covers the basic mechanisms underlying common, rotationally controlled valving technologies; we distinguish between high- and low-pass actuation, depending on whether they release their liquid upon increase or reduction of the spin rate, respectively. In addition to sacrificial barriers, capillary and pneumatic principles, various techniques for priming and thus opening siphon valves are surveyed. After pointing out their numerous synergistical benefits, we designate a full section on siphon valves that run against the pneumatic counter pressure into an outlet chamber that is transiently sealed by a dissolvable-film (DF) barrier. Next, important performance metrics are defined which can guide the design optimization before concluding with a comparison of passive valving techniques for LoaD platforms.

Flow Control

This paper focusses on rotationally controlled valving at the pivot of enhancing functional integration and reliability of centrifugal LoaD systems operating in "stop-and-go" batch mode between subsequent LUOs. We first look into the underlying general hydrostatic model before demonstrating its implementation for common centrifugal valving schemes.

Centrifugal Field

Under rotation at an angular frequency $\omega = 2\pi \cdot \nu$, a particle of mass m, experiences a centrifugal force $F_\omega = m \cdot R \cdot \omega^2$ with its centre of mass located at the radial position R. Within continuum mechanics underlying fluidic systems, we consider the centrifugal force density

$$f_\omega = \varrho \cdot r \cdot \omega^2 \tag{1}$$

Preprints (www.preprints.org) | NOT PEER-REVIEWED | Posted: 27 May 2021 doi:10.20944/preprints202105.0683.v1

which applies to a fluid distribution Λ of density ϱ at a radius r. Other pseudo forces (densities) arising in the non-inertial frame of reference, but of less relevance to this review, are the Euler force (density) $|f_{\mathrm{E}}| = \varrho \cdot r \cdot d\omega/dt$ pointing against the (vector of) the angular acceleration $d\omega/dt$, and the Coriolis force (density) $|f_v| = 2\varrho \cdot \omega \cdot v$ acting on fluids moving at a (local) velocity v [64]; for common centrifugal systems, f_v aligns in the plane of the disc, and perpendicular to the flow, with its direction opposite to the sense of rotation [23, 65].

Liquid Distribution

More generally, we describe microfluidic systems by (contiguous) liquid segments of constant density ϱ, each containing a volume $U_{0,i}$ which assume distributions $\{\Lambda_i(t)\}$ within a given structure Γ at a spin speed $\omega(t)$. In the (quasi) static approximations assumed in this work, i.e., very slow changes $d\omega/dt \approx 0$, we substitute dependency on the time t by ω. Furthermore, for the sake of clarity, we look at each volume distribution $\Lambda_i(\omega)$ individually, for which we apply the notation $\Lambda(\omega)$. In response to a centrifugal field f_ω (1), $\Lambda(\omega)$ assumes a radial extension $\Delta r(t) = r - r_0$ and mean radial position $\bar{r}(\omega) = 0.5 \cdot (r + r_0)$ between its confining upstream and downstream menisci r_0 and r, respectively.

Expressed in cylindrical coordinates with the radial position r and the (potentially disjunct) local cross section $A(r)$, the integral

$$U_0 = \int_{\Lambda(\omega)} dV = \int_{\check{r}(\omega)}^{\hat{r}(\omega)} A(r)dr = \text{const.} \tag{2}$$

corresponds to the total liquid volume U_0 contained in the segment. The conservation of U_0 requires that the liquid volume between their inner- and outermost radial confinements $\check{r}$ and $\hat{r}$, respectively, within the fixed structure of cross-sectional function $A(r)$ is preserved, i.e., $dU_0/d\omega = 0$. While equation (2) captures the general case of a randomly shaped liquid distribution Λ, we will later introduce simplified geometries essentially composed of rectangular cuboids for which the integral over Λ (2) can be replaced by an analytical expression.

Pressure Contributions

Static Pressures

Liquid volumes shape according to the pressure distribution they experience at a given location and time. The rotationally induced pressure head

$$p_\omega = \varrho \cdot \bar{r}\Delta r \cdot \omega^2 \tag{3}$$

derives from (1), and scales with the mean radial position $\bar{r}$ and the radial extension Δr of the liquid segment. The product

$$\bar{r}\Delta r = \frac{1}{2}[r_i + r_0] \cdot [r_i - r_0] = \frac{1}{2}\left[r_i^2 - r_0^2\right] \tag{4}$$

in p_ω (3) can also be expressed by the front and rear radial positions of the menisci r_i and r_0.

The ambient pressure in the atmosphere p_0 and the pneumatic pressure

$$p_V = p_0 \cdot \frac{V_0}{V} \tag{5}$$

of a gas volume that is compressed from an initial volume V_0 at p_0 to $V < V_0$ are of particular interest within this paper. Also relevant to the small feature sizes in centrifugal microfluidics is the capillary pressure

Preprints (www.preprints.org) | NOT PEER-REVIEWED | Posted: 27 May 2021 doi:10.20944/preprints202105.0683.v1

$$p_\Theta = \frac{4\sigma}{D}\cos\Theta \tag{6}$$

as expressed for a liquid of surface tension σ in a channel (of round cross section) with diameter D and the contact angle Θ between the liquid and the surface.

In addition, though not examined in this work, active pressure sources $p(t)$ have been employed in centrifugal LoaD platforms [43, 45, 46, 54, 66-69], as implemented, e.g., by connected pumps, thermo-pneumatic heating or cooling, or chemical reactions providing additional pressure and / or changes in enclosed gas volumes.

Dynamic Effects

In this work we primarily look at hydrostatic approximation $d\omega/dt \approx 0$ when pressure contributions related to flow are neglected. Yet, we briefly mention such dynamic effects. During flow at a volumetric rate Q through a channel with round cross section $A = \pi \cdot (D/2)^2$, a pressure drop

$$p_\mathrm{Q} = \frac{64}{\pi} \cdot \frac{\eta \cdot L \cdot Q}{D} \tag{7}$$

is experienced by a liquid of viscosity η across its axial extension L according to the law of Hagen-Poiseuille. For decelerating a liquid segment volume U travelling at a speed v through a channel of cross section A at a rate dv/dt with $Q = A \cdot v$, a counterpressure

$$p_m = \frac{\varrho \cdot U \cdot dv/dt}{A} \tag{8}$$

is to be delivered by a valve until $Q = 0$.

Hydrostatic Equilibrium

For the batch-mode processing considered in many centrifugal LoaD systems included in this work, flow is intermittently stopped by normally-closed valves, i.e., the term $p_Q \propto Q$ (7) can be neglected. The spatial distribution of the liquid $\Lambda(t)$ is determined by the hydrostatic pressure equilibrium

$$\underbrace{\varrho \cdot \bar{r}\Delta r \cdot \omega^2}_{p_\omega} + p_\rightarrow = p_\leftarrow \tag{9}$$

between $p_\omega \propto \omega^2$ (3), and further contributions $p_\rightarrow$ and $p_\leftarrow$ driving the liquid segment along or against the axial direction of the channel, respectively.

To trigger valving, the equilibrium distribution Λ resulting from (9) is modulated through at least one pressure term via at least one flexibly controllable constituent p_ω, $p_\rightarrow$ or $p_\leftarrow$. If the pressures $p_\rightarrow$ and $p_\leftarrow$ in the hydrostatic equilibrium (9) do not (explicitly) depend on ω, a spin rate

$$\omega = \sqrt{\frac{p_\leftarrow - p_\rightarrow}{\varrho \cdot \bar{r}\Delta r}} \tag{10}$$

can be attributed to a given $\Lambda(\omega)$ of a coherent liquid volume U_0 within a structure Γ as a function of the radial product $\bar{r}\Delta r$ (4), and thus the meniscus positions r_0 and r. A critical frequency $\omega = \Omega$ is defined for $\Lambda(\Omega)$ representing the transition from retention to liquid release, which is linked to a position of the front meniscus $r = r(\Omega)$.

Laboratory Unit Operations

In batch-mode-processing, valves need to close the outlet of an upstream LUO between the points in time of loading T_load and release T_open, while agitating sample or reagents by a frequency protocol $\omega_\mathrm{LUO}(T_\mathrm{load} < t < T_\mathrm{open})$. Most LUOs, such as plasma separation from whole blood, run fastest and most efficiently at high centrifugal field strengths $f_\omega \propto R \cdot \omega^2$ (1) which, for a given layout Γ and

Preprints (www.preprints.org) | NOT PEER-REVIEWED | Posted: 27 May 2021 doi:10.20944/preprints202105.0683.v1

location R, are established at high rates spin rates ω. Liquid retention is thus delineated by a threshold frequency Ω, and a resulting boundary for the field strength $f_\Omega(\omega = \Omega)$ from (1), for which the conditions $\max[\omega_{\mathrm{LUO}}(t)] < \widehat{\Omega}$ or $\min[\omega_{\mathrm{LUO}}(t)] > \breve{\Omega}$ need to be met for high-pass and low-pass valves, respectively.

Furthermore, resilience of the valve to angular acceleration ramps $R \cdot d\omega/dt$ is important to agitate chaotic advection, as it is, for instance, required for liquid-liquid mixing [20], incubation of dissolved biomolecules with surface immobilized capture probes, resuspension of dry-stored reagents, or to support mechanical cell lysis through fixed obstacles or suspended (possibly magnetic) beads [70, 71].

Resulting, inertially induced pressure heads related to p_m (8) need to be factored into the calculation of the retention rates Ω. Also note that for supplying a given moment of inertia of the rotor, such rotational acceleration $(|d\omega) \,/\, dt| > 0$ requires sufficient torque delivered by the spindle motor.

Actuation

For common rotational actuation by the spin rate ω through $p_\omega \propto \omega^2$ (3), the liquid segment is retained upstream of the valve until a certain frequency threshold $\omega = \Omega \in \{\widehat{\Omega}, \breve{\Omega}\}$ is crossed, either surpassed ($\omega > \widehat{\Omega}$) or undershot ($\omega < \breve{\Omega}$) for high-pass and low-pass valves, respectively. In some valving schemes presented later, the rotational actuation may not be well-defined immediately after crossing Ω; proper (high-pass) valving is only assured once a (slightly) higher actuation frequency $\Omega^* > \Omega$ is set.

Alternatively, other pressure contributions in (9) may be changed to prompt valving. Of particular interest of this work will be the venting of the compression chamber to level the pneumatic p_V (5) and atmospheric pressures p_0, i.e., $p_V \mapsto p_0$. Note that in absence inbound pressure gradients, e.g., created by capillary pressure p_Θ (6) or active sources, the centre of gravity $\bar{r}$ of the liquid distribution Λ may only move radially outwards due to the unidirectional nature of the centrifugal field f_ω (1) in the aftermath of valving.

Reliability

Tolerances and Band Width

Due to statistical deviations in its experimental input parameters $\{\gamma_i\}$, the experimentally observed retention frequency Ω spreads over an interval of standard deviation $\Delta\Omega(\{\gamma_i\})$. In the digital twin concept presented here, the spread of the critical spin rate Ω (10)

$$\Delta\Omega(\{\gamma_i\}) = \sqrt{\sum_i \left(\frac{\partial\Omega}{\partial\gamma_i}\Delta\gamma_i\right)^2} \tag{11}$$

can be calculated (and then systematically optimized) by Gaussian error propagation, or through Monte-Carlo methods mimicking a large number of (virtual) test runs, with the tolerances $\Delta\gamma_i$ of the (independent) parameters γ_i.

Using (11), we can directly relate the tolerances $\Delta\Omega$ in critical spin rates Ω (10) to the precision of fundamental experimental parameters for the pipetting or metering ΔU_0, or for vertical and lateral dimensions, e.g., radial positions ΔR, cross sections $\Delta A = \sqrt{(w \cdot \Delta d)^2 + (d \cdot \Delta w)^2}$ and (dead) volumes $\Delta V = \sqrt{(wh \cdot \Delta d)^2 + (dh \cdot \Delta w)^2 + (dw \cdot \Delta h)^2}$, delineating the valve structure Γ.

To avoid premature opening at $\omega < \widehat{\Omega}$ (or $\omega > \breve{\Omega}$ or in low-pass valving), the spin rate ω should be spaced $M \cdot \Delta\Omega$ from the nominal threshold value Ω, where M relates to the desired level of

Preprints (www.preprints.org) | NOT PEER-REVIEWED | Posted: 27 May 2021 doi:10.20944/preprints202105.0683.v1

confidence. The aggregate rate of failure thus calculates to $\{24\%, 7.9\%, 1.7\%, 0.23\%, 0.02\%, 0.0014\%, 2 \times 10^{-5}\%\}$ if the actual spin rate is spaced by $M \cdot \Delta\Omega$ and $M = \{1,2,3,4,5,6,7\}$ from a nominal rate Ω during retention. Hence, in the spirit of Six Sigma, these probabilities imply that above $M \approx 6$ the reliability of this (single) valving step is situated in the range of 1 to 10 defects per million opportunities (DPMO), for $M \geq 7$, DPMOs are practically absent. Consequently, rotationally controlled valves requiring a nominal actuation frequency $\Omega^* > \widehat{\Omega}$ would have to be spaced by $M \cdot \Delta\Omega^*$ from Ω^* for guaranteeing operation at the targetted level of reliability.

Limited Frequency Space for Multiplexing

The maximum degree of multiplexing is limited by the practically allowed range of spin rates ω. At its lower end, the rotationally induced pressure head p_ω (3) still has to dominate capillary effects to keep the liquids at bay, which tends to require $\omega \geq \omega_{\min} \approx 2\pi \cdot 10$ Hz. On its upper end, motor power and concerns of lab safety may demand $\omega \leq \omega_{\max} \approx 2\pi \cdot 60$ Hz. Considering that each CP-DF valve needs to reserve its own (and assuming $\Omega^* \approx \Omega$), non-overlapping band width $M \cdot \Delta\Omega_i$ for assuring correct operation, and the extent of the practical range $\omega_{\max} - \omega_{\min}$, the maximum number of rotationally triggered sequential valving steps N after simultaneous retention of the volumes $\{U_{0,i}\}$ calculates as $\omega_{\max} - \omega_{\min} \geq M \cdot \sum_{i=1}^{N} \Delta\Omega_i$. The simple recipe for maximum exploitation of frequency space for fluidic multiplexing is to minimise $\Delta\Omega_i$ and to stagger the retention rates Ω_i as closely as possible while avoiding overlapping bands $M \cdot \Delta\Omega_i$ between $\omega_{\min}$ and $\omega_{\max}$.

So, for example, a practically allowable ω-range within $\omega_{\min} = 2\pi \cdot 10$ Hz $\leq \omega \leq \omega_{\max} = 2\pi \cdot 60$ Hz and a mean $\Delta\Omega_i/2\pi = 2$ Hz, a 99.99% reliability expressed by $M = 4$ at component level would result in an (average) band width $M \cdot \Delta\Omega_i/2\pi = 4 \cdot 2$ Hz $= 8$ Hz, and thus provide proper operation of 50 Hz$/8$ Hz ≈ 6 concurrently loaded and subsequently triggered CP-DF valving steps i; the reliability at system level would amount to $0.9999^3 \approx 99.97\%$. For $M = 2$, we could halve the width of the required frequency envelope to provide space for of 50 Hz$/4$ Hz ≈ 12 frequency bands, at the expense of a drop in system-level robustness to $0.95^3 \approx 85.7\%$. Note that for the sake of simplicity, these back-of-the-envelope calculations were based on an even width $\Delta\Omega_i$ of the forbidden frequency spread, which they actually tend to broaden towards larger spin rates ω.

Multiplexing

The digital twin approach will support the design of LoaD structures implementing multiplexed liquid handling protocols. Key flow control capabilities are the simultaneous and sequential release of several liquid volumes $\{U_{i,j}\}$ loaded to rotational valving structures $\{\Gamma_{i,j}\}$ located at radial positions $\{R_{i,j}\}$. During their retention, the common spin rate needs to follow $\omega < \min\{\Omega_i - 0.5 \cdot M \cdot \Delta\Omega_i\}$ for high-pass and $\omega > \max\{\Omega_i + 0.5 \cdot M \cdot \Delta\Omega_i\}$ for low-pass valves. The order of release by venting simply relates to the sequence of the removal of the seals.

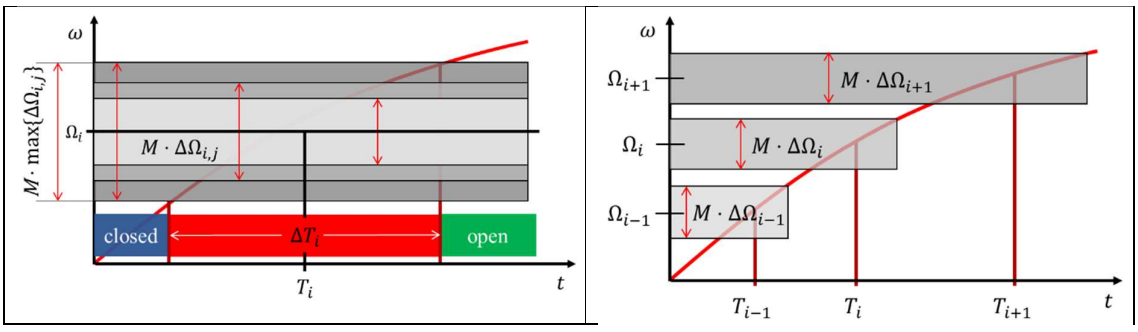

Preprints (www.preprints.org) | NOT PEER-REVIEWED | Posted: 27 May 2021 doi:10.20944/preprints202105.0683.v1

(a) Simultaneous actuation.	(b) Sequential actuation.

Figure 1 Fluidic multiplexing of rotationally actuated high-pass valving on the LoaD platform. (a) Robust concurrent actuation of valves $\{j\}$ of a step i sharing the critical spin rate Ω_i at a time T_i requires lifting of the spin rate ω across the interval of width $M \cdot \max\{\Delta\Omega_{i,j}\}$, which takes a time span ΔT_i. (b) In serial actuation of steps $\{i\}$, the frequency intervals $\{M \cdot \Delta\Omega_i\}$ around the actuation frequencies $\{\Omega_i\}$ need to be separated in order assure the correct order of release at times $\{T_i\}$.

For rotationally actuated simultaneous release of high-pass valves $\{j\}$ at the time T_i (Figure 1a), the spin rate $\omega(t)$ needs cross a zone $M \cdot \max\{\Delta\Omega_{i,j}\}$ centred at the common, nominal release rate Ω_i within an interval ΔT_i. For sequential actuation of valves $\{i\}$ at times $\{T_i\}$ (Figure 1b), the critical spin rates $\{\Omega_i\}$, with $\Omega_{i-1} < \Omega_i$ and $T_{i-1} < T_i$, must be spaced so that their tolerance intervals $\{M \cdot \Delta\Omega_i\}$ do not overlap.

Basic Centrifugal Flow Control Schemes

Sacrificial Barriers

Apparently straight-forward implementation of normally-closed valves are removable materials for intermittently blocking liquids and gases. Various types of such sacrificial-barrier valves have been developed [72-74]. However, most of them require external actuation by an instrument-based module. Examples are wax plugs [50] melted by irradiation and barrier films that are disrupted by knife cutters (xurography) [48], pressure sources, heat [50] or laser ablation [53].

In rotationally controlled LoaD systems that are mainly considered here, a membrane or its seal open these sacrificial barriers once the rotationally induced pressure head $p_\omega(R_{\text{seal}}) \propto R_{\text{seal}} \cdot \Omega_{\text{seal}}^2 > p_{\text{seal}}$ (3) applying at the location of the seal R_{seal} exceeds a minimum threshold p_{seal}. Yet, the sensitivity of the release frequency Ω_{seal} on manufacturing tolerances tends to result in a large band width $\Delta\Omega_{\text{seal}}$.

More recently, dissolvable films (DFs) that selectively disintegrate of become permeable upon contact with a specific solvent, e.g., of aqueous or organic nature, have been used for flow control [32, 47, 61, 75]. It has been shown for a wider range of assays that the dissolved molecules do not interfere with bioanalytical protocols or detection, and could be effectively removed from their flow path into a side chamber under the prevalent laminar flow conditions. To provide timing of their upstream LUOs according to the programmable spin protocol $\omega(t)$, DF valves have been combined with centrifugo-pneumatic valving.

Centrifugo-Capillary Burst Valves

Hydrophobic constrictions and also hydrophilic expansions with sharply defined edges have been frequently used in centrifugal microfluidic system to stop the flow at a well-defined (axial) position $r = R$ along a channel [10, 37, 64, 76]. For a liquid segment driven by the centrifugal pressure p_ω (3) down a channel, such barriers exert a net counterpressure $p_\leftarrow$ composed of the capillary pressures p_Θ (6) of its radially outbound, front and rear menisci $p_{\Theta,\text{front}}$ and $p_{\Theta,\text{rear}}$, respectively (Figure 2).

Preprints (www.preprints.org) | NOT PEER-REVIEWED | Posted: 27 May 2021 doi:10.20944/preprints202105.0683.v1

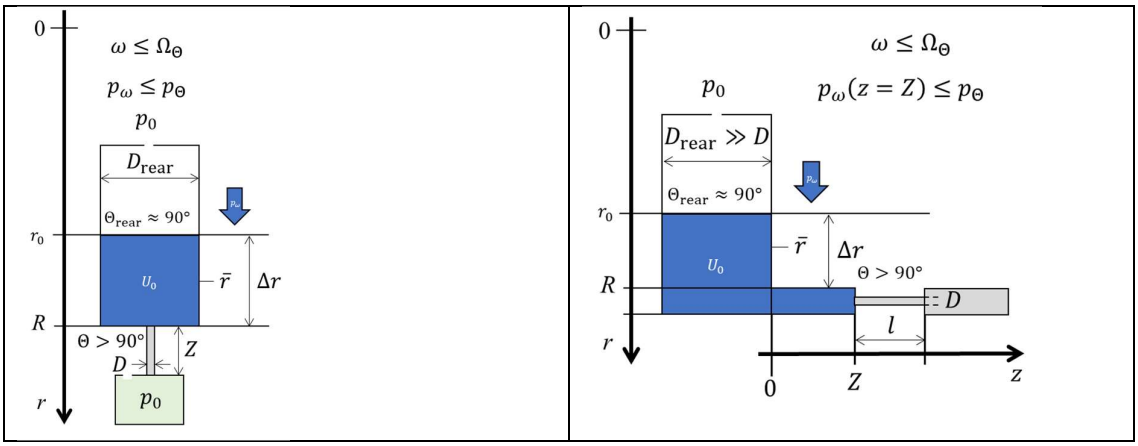

Figure 2 Centrifugo-capillary burst valve (not to scale). In this hydrophobic constriction, a centrifugal pressure head $p_\omega \propto \bar{r}\Delta r$ (3) runs against the capillary counterpressure $p_\leftarrow = p_\Theta$ (6) calculated by the contact angles $\Theta > 90°$ and $\Theta_{\mathrm{rear}} \approx 90°$ and their channel diameters $D \ll D_{\mathrm{rear}}$ for their front and rear menisci, respectively. The valve stays closed until a critical spin rate Ω_Θ (12) is surpassed. (Left) Radial alignment. (Right) Isoradial alignment where radial "squeezing" of the liquid on the isoradial outlet may become an issue.

In the hydrostatic approximation, a threshold frequency for a hydrophobic constriction

$$\Omega_\Theta = \sqrt{\frac{4\sigma}{\varrho \cdot \bar{r} \cdot \Delta r}\left(\frac{\cos\Theta_{\mathrm{rear}}}{D_{\mathrm{rear}}} - \frac{\cos\Theta}{D}\right)} \approx \sqrt{-\frac{4\sigma}{\varrho \cdot \bar{r} \cdot \Delta r}\frac{\cos\Theta}{D}} \tag{12}$$

results from insertion of $p_\leftarrow = p_\Theta$ and $p_\rightarrow = 0$ (6) into (10), which needs to be surpassed for the liquid volume to progress to $r > R$. Often the hydrophobic barriers are designed with $D/D_{\mathrm{rear}} \ll 1$ and / or $\Theta_{\mathrm{rear}} \approx 90°$, so that the contribution from the rear meniscus becomes negligible. Note that with $\Theta > 90°$ for a hydrophobic coating, $\cos\Theta < 0$. Assuming a density $\varrho \approx 1000\ \mathrm{kg\ m^{-3}}$ and surface tension $\sigma = 75\ \mathrm{mN\ m^{-1}}$ of water, its contact angle $\Theta \approx 120°$ with Teflon, a mean radial position $\bar{r} = 3\ \mathrm{cm}$ and radial extension $\Delta r = 1\ \mathrm{cm}$, a constriction diameter $D = 100\ \mu\mathrm{m}$, we obtain a threshold spin rates in the region of $\Omega_\Theta/2\pi \approx 10\ \mathrm{Hz}$. Note that at these low spin rates $\omega < \Omega_\Theta$, detachment of a droplet as outlined later in the context of the centrifugo-pneumatic valve in (15) is not expected as $\Omega_\Theta \ll \Omega_{\mathrm{drop}}$.

Hydrophilic expansions also produce a barrier to flow. However, their retention frequencies Ω tend to be much smaller, and sensitively depend on the exact shape, surface tension σ and contact angle Θ at the liquid-gas interface. Such hydrophilic expansions are thus often used for transient pinning the meniscus or shaping the front of creeping flows, e.g., during capillary priming of microfluidic chips.

Note that capillary barriers do not to curb evaporation which leads to volume loss and humidity into the connected fluidic network; they are thus unsuitable for longer-term liquid storage. Also, capillary barriers often involve significant manufacturing and assembly challenges as all four walls, with one of them usually created by a flat lid, need to display well-defined and localized coatings. Otherwise, retention rates Ω might shift, or flow might just be delayed, instead of being stopped as required for proper batch-mode processing.

Centrifugo-Pneumatic Burst Valves

Pneumatic Retention

For rotational flow control, the centrifugal pumping by p_ω (3) can be counteracted by a pneumatic pressure $p_\leftarrow = p_V$ (5) arising from the compression of a gas volume enclosed at the downstream end. As outlined in Figure 3a, this counter pressure p_V is increased from its initial value $p_0 + \delta p_0 =$

Preprints (www.preprints.org) | NOT PEER-REVIEWED | Posted: 27 May 2021 doi:10.20944/preprints202105.0683.v1

$p_0 \cdot (1+\chi)$ at $\omega \approx 0$ by reduction of the gas volume. The small offset δp_0 with $\delta p_0/p_0 = \chi \ll 1$ of the gas pressure at the volume $V_C + A \cdot Z$ represents deviations from the hydrostatic approximation attributed to dynamic effects during filling. It may be explained by an additional volume that is drawn with the flow into the compression chamber, and needs to be quantified empirically, or by advanced simulation.

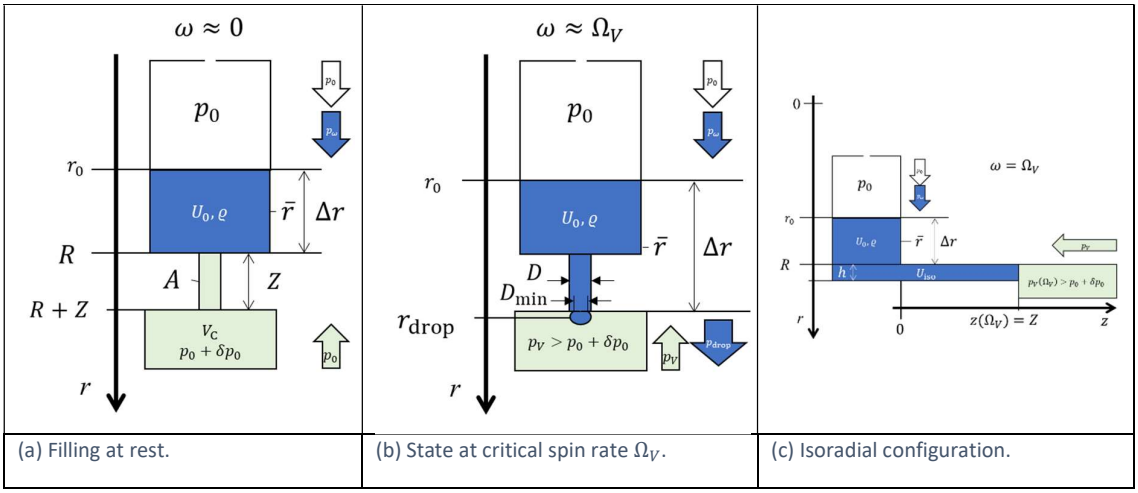

(a) Filling at rest. (b) State at critical spin rate Ω_V. (c) Isoradial configuration.

Figure 3 Centrifugo-pneumatic valving (not to scale). (a) At rest ($\omega \approx 0$), the liquid stops at $r = R$ in front of the radial outlet of length Z and a sufficiently narrow cross section A , which is followed by a compression chamber. At this point the gas volume V_C is at atmospheric pressure p_0, plus a small contribution δp_0 with $\chi = \delta p_0/p_0 \ll 1$ linked to (dynamic) filling effects. (b) At a critical spin rate Ω_V, the meniscus protrudes to $r = R + Z$ at the transition to the pneumatic chamber. Now the pneumatic counterpressure has increased to $p_V = p_0 \cdot (1+\chi) \cdot (V_C + A \cdot Z)/V_C$, and a droplet of volume $V_{drop} \approx (4/3)\pi(D/2)^3$ located at $r = r_{drop} \approx R$ emerges from the orifice. Centrifugo-pneumatic valving is triggered once the weight force $F_m = V_{drop} \cdot f_\omega$ (1) exceeds the counteracting surface tension force $F_\sigma = \pi D_{min} \cdot \sigma$ at its minimum diameter $D_{min} = D/\kappa$ with $\kappa > 1$. While the exact dynamics are unclear and hard to quantify, it is assumed that the hydrodynamic agitation caused by the detaching droplet disrupts the integrity of the liquid plug, thus causing successive release of the entire liquid into the compression chamber while gas escapes in the reverse direction to atmosphere. (c) CP valving with an isoradial outlet pinned at $r = R$. A minimum liquid volume $U_0 \geq U_{iso}$ is required for generating a $\Delta r > 0$ and thus $p_\omega > p_V(\Omega_V)$ for opening. Toward high field strength f_ω (1), the front meniscus might get distorted.

At $\omega = \Omega_V$ (Figure 3b), the original gas volume is reduced by $A \cdot Z$ to V_C, thus increasing its pressure to $p_V = p_0 \cdot (1+\chi) \cdot (V_C + A \cdot Z)/V_C$ (5). The cross section A needs to be sufficiently small so that surface tension sustains "piston-like" characteristics of the liquid plug. Under these conditions, we set

$$p_{\leftarrow} = p_V = p_0 \cdot (1+\chi) \cdot \left(1 + \frac{A \cdot Z}{V_C}\right) \tag{13}$$

and $p_{\rightarrow} = p_0$ to obtain a critical spin rate (10)

$$\Omega_V = \sqrt{\frac{p_0}{\varrho \cdot \bar{r} \cdot \Delta r} \cdot \left[(1+\chi) \cdot \left(1 + \frac{A \cdot Z}{V_C}\right) - 1\right]} \approx \sqrt{\frac{p_0}{\varrho \cdot \bar{r} \cdot \Delta r} \cdot \frac{A \cdot Z}{V_C}} \tag{14}$$

for positioning the front meniscus at its end at $r = R + Z$. For typical values, $\bar{r} \approx R = 3$ cm, $\Delta r = 1$ cm, a volume ratio $A \cdot Z/V_C \approx 1/10$ and $\delta p_0 \approx 0$, this approximation provides a release threshold in the region of $\Omega/2\pi \approx 30$ Hz.An isoradial variant of the valve (Figure 3c) tends to result in a tilting the surface of the meniscus, thus compromising the validity of the formula for Ω_V (14).

Compensation of Ambient Pressure

Note that Ω_V (14) depends on the local atmospheric pressure p_0, which shifts with local altitude and weather (see also Figure 4). Yet, these fluctuations would normally remain constant over time spans of typical experimental protocols. The actual value of p_0 may thus be measured by a sensor, e.g., as

Preprints (www.preprints.org) | NOT PEER-REVIEWED | Posted: 27 May 2021 doi:10.20944/preprints202105.0683.v1

attached to the instrument, for adjusting the spin protocol $\omega(t)$ induced by this systematic deviation to the new retention rates Ω_V (14).

The main systematic error in the threshold spin rate Ω_V (14) is introduced by its dependence on the actual ambient (atmospheric) pressure p_0' from its nominal (standard) value $p_0 = 1013.25\ \mathrm{hPa}$ at sea level, which remains rather constant at a given geolocation, and over the typical course of a bioassay of minutes to an hour. By timely local measurement of p_0', the spin protocol $\omega(t)$ can be flexibly adjusted by the factor $\sqrt{\Delta p_0'/p_0}$ to compensate the dependency $\Omega = \Omega(p_0')$.

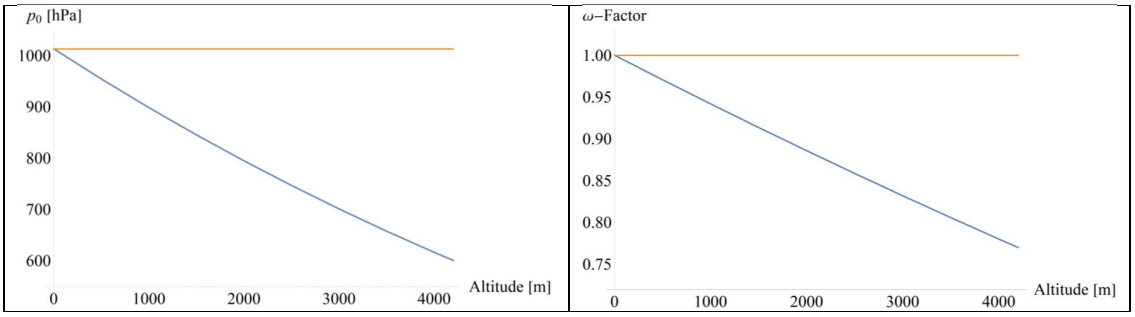

Figure 4 Variation in the atmospheric pressure p_0. (Left) Barometric formula quantifies the decrease in atmospheric pressure from sea level to roughly the limit of habitable space on earth at roughly 4000 m altitude. (Right) Compensation factor of spin rate ω for altitude adjusted (standard) pressure. For the given example, the critical spin rate would reduce by about 20% from $\Omega/2\pi = 25\ \mathrm{Hz}$ at sea level to about 20 Hz in high altitude. In general, any known local pressure p_0', either caused by altitude or weather, can be compensated by adjusting the spin rate ω according to $\sqrt{p_0'/p_0}$ (23). Similar adjustments can also be applied for $\chi > 0$.

While it is subject to fluctuations of a few percent depending on climate and (not extreme) weather conditions, p_0 shows significant variation with local elevation. Figure 4 shows the reduction of the atmospheric pressure with altitude up to the highest settlements on earth by about 30% (left), and the required compensation of the spin rate ω to assure proper retention of liquid volumes by about 3%, 6%, 9% and 12% at 500 m, 1000 m, 1500 m and 2000 m, respectively. Similar considerations can be applied for the compensation of $\chi \neq 0$. Note that a tolerance-forgiving design would then make sure that the (lower) centrifugal field f_ω (1) would still be sufficient to carry out the upstream LUO, possibly by also extending its related time interval in the spin protocol $\omega(t)$.

Droplet Release

To effectuate basic centrifugo-pneumatic valving, a droplet of volume $V_{\mathrm{drop}} \approx (4/3)\pi(D/2)^3 \ll V_{\mathrm{C}}$ located at the radial position r_{drop} is pulled by the centrifugal force $F_m = V_{\mathrm{drop}} \cdot f_\omega = V_{\mathrm{drop}} \cdot \varrho \cdot r_{\mathrm{drop}} \cdot \omega^2$ (1) out of the orifice to the compression chamber. While the exact mechanism is somewhat obscure, we consider a simplified model akin to goniometric measurement of surface tension; detachment of the hanging droplet is suppressed until its surface tension force $F_\sigma = \sigma \cdot \pi D_{\mathrm{min}}$ at its minimum cross section of diameter $D_{\mathrm{min}} = D/\varepsilon$ with $\varepsilon > 1$ cannot sustain its weight force F_m anymore. This model leads to a spin rate

$$\Omega_{\mathrm{drop}} \approx \sqrt{\frac{\sigma \cdot \pi D_{\mathrm{min}}}{\varrho \cdot (4/3)\pi(D/2)^3 \cdot r_{\mathrm{drop}}}} \approx \frac{1}{D}\sqrt{\frac{6\sigma}{\varepsilon \cdot \varrho \cdot (R+Z)}} \tag{15}$$

for droplet release with $r_{\mathrm{drop}} \approx R + Z$ and $D_{\mathrm{drop}} \approx D$.

Inserting typical values $D \approx 200\ \mu\mathrm{m}$, $\sigma \approx 75\ \mathrm{mN\ m^{-1}}$, $\varepsilon \approx 1.5$, $\varrho \approx 1000\ \mathrm{kg\ m^{-3}}$ and $R \approx 3\ \mathrm{cm}$ in (15), we obtain $\Omega_{\mathrm{drop}}/2\pi \approx 80\ \mathrm{Hz}$. This very coarse "back of the envelope" estimate reveals that the threshold spin rate for droplet release Ω_{drop} (15) sensitively depends on the diameter of the outlet D.

Preprints (www.preprints.org) | NOT PEER-REVIEWED | Posted: 27 May 2021 doi:10.20944/preprints202105.0683.v1

Rotational Actuation

Followingly, droplet release triggering the opening of centrifugo-pneumatic valves essentially proceeds at frequencies

$$\Omega_{\mathrm{cpv}} = \min\{\Omega_V, \Omega_{\mathrm{drop}}\} \tag{16}$$

and may be associated with rather large uncertainties $\Delta\Omega_{\mathrm{cpv}}$ caused by effects that are hard to quantify by simple modelling.

It is surmised that the detachment of a (first) hanging drop above Ω_{cpv} (16) severely disrupts the surface of the liquid plug, so that a certain portion of the compressed air can escape through the outlet and thus gradually vent the compression chamber. This partial venting step has a bigger impact on the pneumatic counter pressure p_V (5) than the loss of liquid volume to the chamber on the radial product $\bar{r}\Delta r$ in p_ω (3). Consequently, more liquid will penetrate into the compression chamber to gradually complete the transfer. Such step-wise liquid release has indeed been experimentally observed in the region $\omega \approx \Omega_{\mathrm{cpv}}$. It was accompanied by a large spread $\Delta\Omega_{\mathrm{cpv}}$, which may reflect the sensitivity of Ω_{drop} (15) to is experimental input parameters.

Their comparatively high burst frequencies Ω_{cpv} in (16), combined with their large spread $\Delta\Omega_{\mathrm{cpv}}$ make such basic centrifugo-pneumatic flow control schemes mainly suitable for final valving steps into an end chamber, e.g., for aliquoting of liquid sample or reagents into detection chambers [77]. Furthermore, centrifugo-pneumatic valving requires powerful spindle motors, aerodynamic optimization and mechanically well-balanced rotors, and may raise concerns about lab safety.

Venting

An alternative actuation mechanism for these CP-valves is given by venting the compression chamber $V_{\mathrm{C}} \mapsto \infty$ leading to $p_V \mapsto p_0$ (). While this principle would allow high retention frequencies Ω_V (14), and thus vigorous agitation for its upstream LUO (Figure 5a), it turned out to be challenging to provide a conceptually simple mechanism for perforating the pneumatic chamber during high-speed rotation (Figure 5b) . Especially in the context of “event-triggered” valving concepts [62, 63, 78], venting of compression chambers sealed dissolvable film (DF) membranes through arrival of a sufficient volume of ancillary liquids at strategic locations has been implemented (Figure 5c).

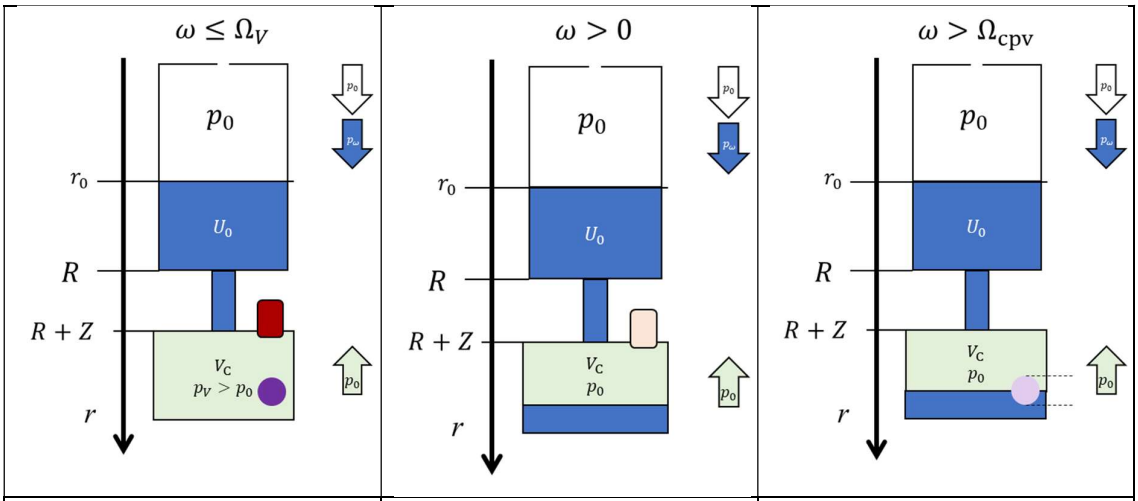

(a) Retention phase. (b) Venting through membrane. (c) Venting through dissolvable film.

Figure 5 Centrifugo-pneumatic valving by venting. (a) Below the retention rate $\omega \leq \Omega_V$ (14), the liquid is kept outside the pneumatic chamber which is sealed by a gas-impermeable membrane or dissolvable film (DF). (b) Upon venting, the pneumatic counter pressure p_V converges to the atmospheric pressure p_0, thus releasing the liquid for $\omega > 0$. (c) For this

Preprints (www.preprints.org) | NOT PEER-REVIEWED | Posted: 27 May 2021 doi:10.20944/preprints202105.0683.v1

high-pass valve, liquid enters the compression chamber after the retention frequency is passed at $\omega > \Omega_{\mathrm{cpv}}$ (16). After a sufficient volume $U_{\mathrm{DF}} = \beta \cdot V_{\mathrm{C}}$ with $0 < \beta < 1$ has entered the compression chamber of volume V_{C}, the liquid wets and thus opens the DF, liquid can flow out at $\omega > 0$ through an outlet, e.g., located in a lower layer which is connected through a vertical underneath the DF.

Centrifugal Siphon Valving

Layout and Liquid Distribution

For understanding the core principle underlying centrifugal siphoning, Figure 6 displays a basic design Γ with an inner reservoir of cross section A_0, a bottom at R which is connected by an isoradial segment of volume U_{iso} radial, length L_{iso} and height h_{iso} to a siphon channel of (constant) cross section $A < A_0$. Its isoradial channel at the crest point $R_{\mathrm{crest}} = R - Z$ has a volume capacity U_{crest}, axial length L_{crest} and radial height h_{crest}. The radially directed outlet channel of volume U_{out} extends between R_{crest} and the final receiving chamber starting at $R_{\mathrm{cham}} > R$. We consider adjustment of the liquid distribution $\Lambda(\omega)$ between (hydrostatic) equilibria $p_\omega(\omega) + p_z(\omega) = 0$ with p_ω (3) and an axially directed pressure head $p_z = p_{\rightarrow} - p_{\leftarrow}$, with forward and reverse contributions $p_{\rightarrow}$ and $p_{\leftarrow}$, respectively, in response to a (slowly) changing spin rate $\omega = \omega(t)$.

A first equilibrium distribution $\Lambda(\Omega)$ can be found in the inbound segment at $r_1 = r(\Omega)$ with $R_{\mathrm{crest}} < r_1 < R$ for a loaded liquid volume $U_0 > U_{\mathrm{iso}}$. Optionally, the meniscus in the inbound segment may be "pinned" to a fixed target position r_1 by a small capillary barrier or by a widening of the channel cross section.

A second critical point $R_{\mathrm{crest}} < r_2 = r(\Omega^*) < R_{\mathrm{cham}}$ in the outbound channel beyond which any further increase in $\Delta r = r_2(\omega) - r_0(\omega)$, e.g., induced by topping up a liquid volume U_Δ or modulating ω, leads to an increase in the pumping force p_ω (3). Different types of siphon valves can be categorized by their priming mechanism to assure $p_\omega(\omega) + p_z(\omega) > 0$ for migrating between $r_1 = r(\Omega)$ and $r_2 = r(\Omega^*)$.

Priming

In volume addition mode (Figure 6a), priming is triggered by topping up U_0 with $U_\Delta > 0$. Figure 6a shows the simplest case for $p_z = 0$, so pumping initiates at any spin rate $\omega > 0$ once the outlet channel is reached to assure $\Delta r > 0$, so the liquid level on the radially outbound channel has fallen below the inner meniscus in the inlet reservoir.

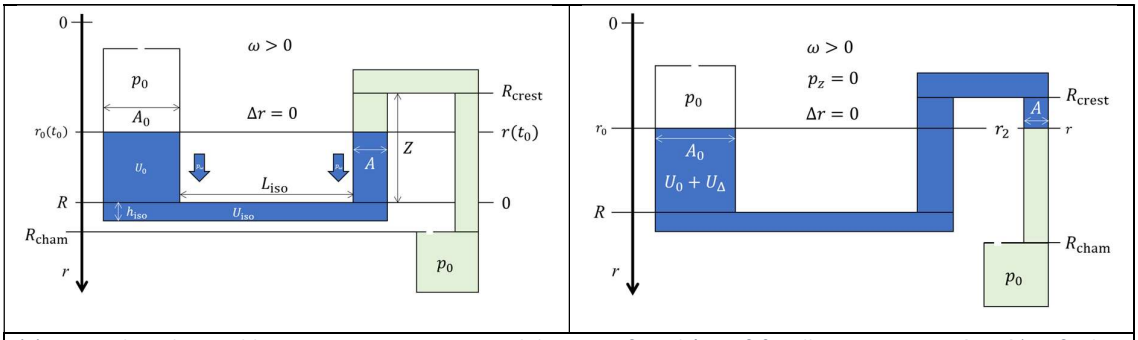

(a) Priming by volume addition. For $p_{\rightarrow} = p_{\leftarrow} = p_0$, and thus $p_z = 0$, and $\Delta r = 0$ for all spin rates $\omega > \Omega = \Omega^* = 0$. The front meniscus resides at r_1 in the inbound segment for all liquid volumes U_0 in $0 < U_0 - U_{\mathrm{iso}} < (A_0 + A) \cdot Z$. An amount $U_\Delta > 0$ with $U_0 + U_\Delta = (A_0 + A) \cdot Z + U_{\mathrm{iso}} + U_{\mathrm{crest}} + A \cdot (r_2 - R_{\mathrm{crest}})$ needs to be added to shift the meniscus to the outbound section. The conservation of liquid volume U_0 between Ω and Ω^*demands $U_0 = A_0 \cdot [R - r_0(\Omega)] + U_{\mathrm{iso}} + A \cdot [R - r_1(\Omega)] = A_0 \cdot [R - r_0(\Omega^*)] + U_{\mathrm{iso}} + A \cdot Z + U_{\mathrm{crest}} + A \cdot [R_{\mathrm{crest}} - r_2(\Omega^*)] - U_\Delta$. After a critical position $r_2 = r_0 > R_{\mathrm{crest}}$ is reached, $\Delta r > 0$ for all $\omega > 0$ without further volume addition, so centrifugally driven forward pumping sets in.

Preprints (www.preprints.org) | NOT PEER-REVIEWED | Posted: 27 May 2021 doi:10.20944/preprints202105.0683.v1

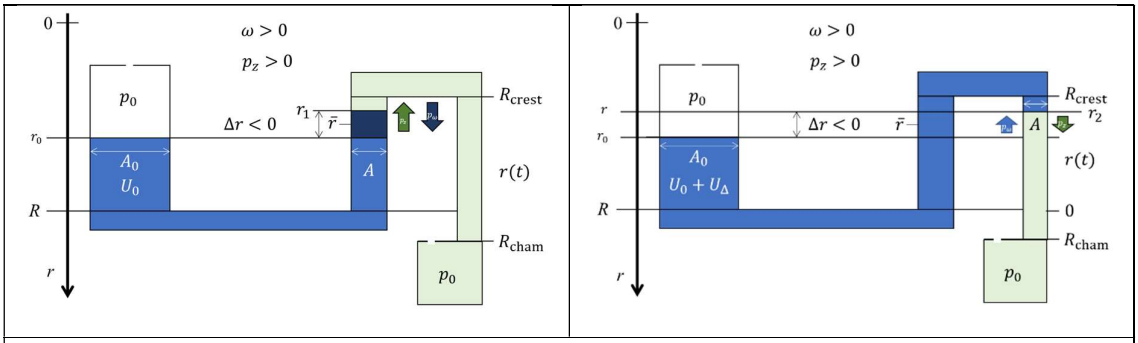

(b) For priming in low-pass siphon valves, $p_z > 0$, $\Delta r < 0$ and $\Omega^* < \Omega$, and $U_\Delta = 0$.

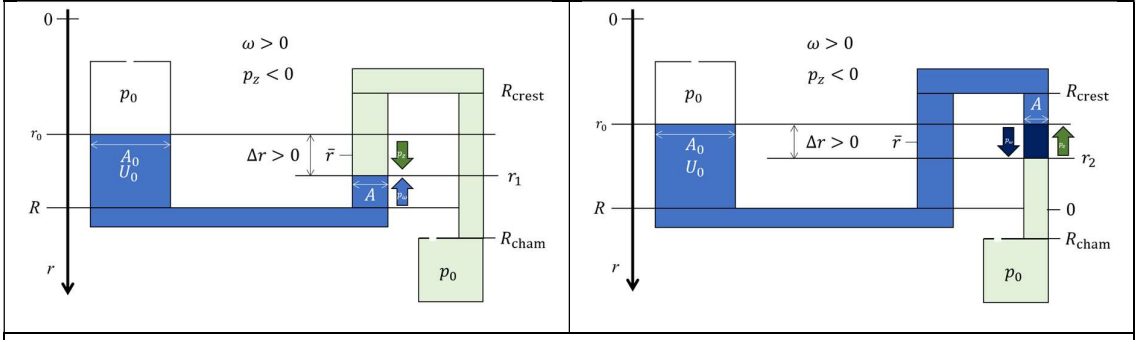

(c) For high-pass valves, $p_z < 0$, $\Delta r > 0$ and $\Omega^* > \Omega$, and $U_\Delta = 0$.

Figure 6 Centrifugally controlled siphon valving with distributions Λ for retention (left) and release (right) (not to scale). The layout Γ features an inlet reservoir of cross section A_0 and a bottom at R, and isoradial outlet of length L_{iso}, radial height h_{iso} and volume U_{iso}. The following siphon channel of cross section $A \ll A_0$ starts with an inbound segment of radial length Z between R and a crest point $R_{\text{crest}} = R - Z < R$, an inner isoradial channel of axial length L_{crest}, radial height h_{crest} and volume U_{crest}, and an outlet channel of volume U_{out} along the interval $R_{\text{crest}} < r < R_{\text{cham}}$ leading to a collection chamber at $R_{\text{cham}} > R$. The ambient pressure p_0 applies to all vented chambers. The menisci confining the liquid U_0 in the inlet, the inbound and outbound sections are r_0, r_1 and r_2, respectively. A net centrifugal pressure $p_\omega \propto \Delta r \cdot \omega^2$ (3) with $\Delta r(\omega) = r_i(\omega) - r_0(\omega)$ and $i \in \{1,2\}$ plus an axially directed pressure difference $p_z = p_\rightarrow - p_\leftarrow$, which is composed of forward and backwards contributions $p_\rightarrow$ and $p_\leftarrow$, act on the liquid. A first critical retention frequency Ω can be evaluated to establish with $p_\omega(r_1) + p_z(r_1) = 0$ in the inbound segment. A second critical position r_2 can be found within the outlet segment at a second spin rate Ω^* at $p_\omega(\Omega^*) + p_z(\Omega^*) = 0$, possibly after adding a liquid volume U_Δ to U_0. Valving is practically possible if the calculated Ω and Ω^* reside within the frequency envelope between ω_{min} and ω_{max}, and the radial positions r_0, r_1 and r_2 within their allowed radial intervals $R_{\text{min}} < r_0 < R$, $R_{\text{crest}} < r_1 < R$ and $R_{\text{crest}} < r_2 < R_{\text{out}}$.,

For low-pass siphon valving in Figure 6b, $p_z > 0$ and $U_\Delta = 0$, a threshold $\Omega^* < \Omega$ can be determined to guarantee pumping for $\omega < \Omega^*$. Conversely, the basic high-pass siphoning concept illustrated in Figure 6c open when $p_\omega + p_z > 0$ along the entire path of the front meniscus r_2 to the end of the outlet at R_{cham}, and during release into the chamber.

Note that, for a given design Γ, the liquid distributions $\Lambda(\omega)$ need to obey the continuity of volume as expressed by $A_0 \cdot [R - r_0(\Omega)] + U_{\text{iso}} + A \cdot [R - r_1] = A_0 \cdot [R - r_0(\Omega^*)] - U_{\text{iso}} + A \cdot Z + U_{\text{crest}} + A \cdot [r_2 - R_{\text{crest}}] - U_\Delta$. Furthermore, for valid solutions $\Lambda(\Omega)$ and $\Lambda(\Omega^*)$, the menisci at r_i with $i \in \{0, 1, 2\}$ need be situated within the corridors $R_{\text{min}} < r_0 < R$, $R_{\text{crest}} < r_1 < R$ and $R_{\text{crest}} < r_2 < R_{\text{cham}}$, while $\omega_{\text{min}} \leq \omega \leq \omega_{\text{max}}$ needs to hold for the critical spin rates $\omega = \Omega$ and $\omega = \Omega^*$.

Pneumatic Priming

The same principle used as counterpressure $p_\leftarrow$ for the basic pneumatic valving mode (Figure 3) can also be implemented for priming the siphon valve [58, 79], i.e., $p_\rightarrow = p_V$ (5). To this end, a side chamber of dead volume V_{side} is laterally connected to the upstream inlet reservoir (Figure 7). In a hypothetical multi-stage procedure, a first liquid volume U_{iso} is loaded at small $\omega \approx 0$ (Figure 7a). At

Preprints (www.preprints.org) | NOT PEER-REVIEWED | Posted: 27 May 2021 doi:10.20944/preprints202105.0683.v1

this stage, a gas volume V_{side} of the same size as the side chamber is disconnected from the main valving structure by the incoming liquid. This gas volume V_{side} experiences a pressure $p_0 + \delta p_0$, with $\delta p_0 = \chi \cdot p_0$ and $\chi \ll 1$.

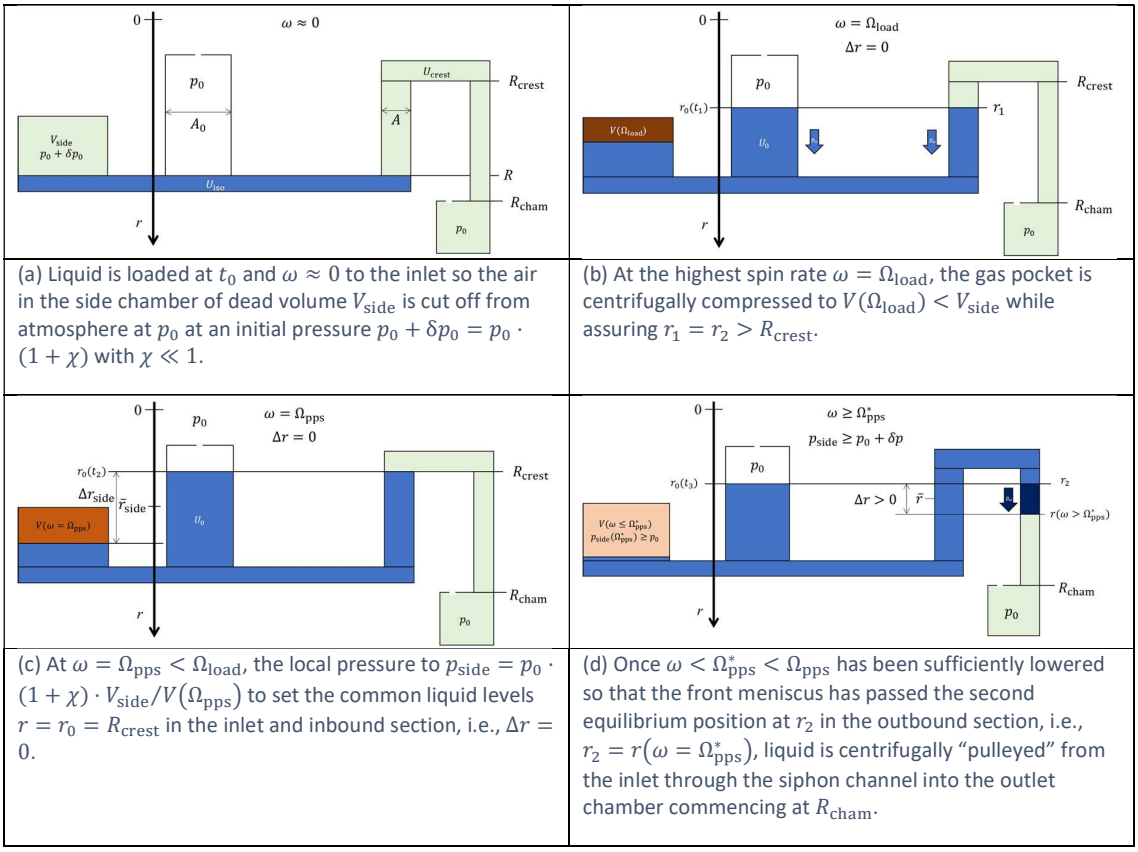

(a) Liquid is loaded at t_0 and $\omega \approx 0$ to the inlet so the air in the side chamber of dead volume V_{side} is cut off from atmosphere at p_0 at an initial pressure $p_0 + \delta p_0 = p_0 \cdot (1 + \chi)$ with $\chi \ll 1$.

(b) At the highest spin rate $\omega = \Omega_{\text{load}}$, the gas pocket is centrifugally compressed to $V(\Omega_{\text{load}}) < V_{\text{side}}$ while assuring $r_1 = r_2 > R_{\text{crest}}$.

(c) At $\omega = \Omega_{\text{pps}} < \Omega_{\text{load}}$, the local pressure to $p_{\text{side}} = p_0 \cdot (1 + \chi) \cdot V_{\text{side}}/V(\Omega_{\text{pps}})$ to set the common liquid levels $r = r_0 = R_{\text{crest}}$ in the inlet and inbound section, i.e., $\Delta r = 0$.

(d) Once $\omega < \Omega^*_{\text{pps}} < \Omega_{\text{pps}}$ has been sufficiently lowered so that the front meniscus has passed the second equilibrium position at r_2 in the outbound section, i.e., $r_2 = r(\omega = \Omega^*_{\text{pps}})$, liquid is centrifugally "pulleyed" from the inlet through the siphon channel into the outlet chamber commencing at R_{cham}.

Figure 7 Pneumatic siphon priming with $p_z = p_{\rightarrow} = p_V$ and a vented outlet, i.e., $p_{\leftarrow} = p_0$ (not to scale).

In the next step (Figure 7b), the spin rate is steeply increased to Ω_{load} for shrinking the enclosed gas volume to $V(\Omega_{\text{load}}) < V_{\text{side}}$ while $r_0 = r_1 = r > R_{\text{crest}}$. After setting the critical retention rate to $\omega = \Omega_{\text{pps}} < \Omega_{\text{load}}$ (Figure 7c), the enclosed gas expands to $V(\omega = \Omega_{\text{pps}})$ defined by $r_1 = r_0 \leq R_{\text{crest}}$, and thus just still preventing overflow. At $\omega = \Omega^*_{\text{pps}} < \Omega_{\text{pps}}$ (Figure 7d), the liquid level reaches above the crest channel, i.e., $r_1 \leq R_{\text{crest}}$. Mainly depending on the cross section of the crest and outlet sections, liquid is either transferred into the outer chamber at R_{cham} by overflow of liquid pulley mechanisms.

In more detail, the gas pressure in the side chamber amounts to

$$p_{\text{side}}(\omega) = \varrho \cdot \bar{r}_{\text{side}} \Delta r_{\text{side}} \cdot \omega + p_0 \cdot (1 + \chi) \cdot \frac{V_{\text{side}}}{V(\omega)} \tag{17}$$

with the mean value and difference $\bar{r}_{\text{side}}$ and Δr_{side} of the liquid levels between the inlet and the side chamber. For such pneumatic priming of the siphon to work, i.e., to reach $\Delta r > 0$, the geometry Γ and liquid volume U_0 have to be configured so

$$V(\Omega^*_{\text{pps}}) - V(\Omega_{\text{pps}}) \geq [r_1(\Omega_{\text{pps}}) - R_{\text{crest}}] \cdot (A_0 + A) + U_{\text{crest}} \tag{18}$$

holds for the gas volume displaced from the side chamber into the main structure while reducing the spin rate ω from Ω_{pps} to Ω^*_{pps}.

Preprints (www.preprints.org) | NOT PEER-REVIEWED | Posted: 27 May 2021 doi:10.20944/preprints202105.0683.v1

Capillary Priming

For priming by capillary action, the outlet may be hydrophilically coated to provide a (constant) contact angle $0 < \Theta < 90°$ at all interfacial surfaces, and hence $p_z = p_{\rightarrow} = p_\Theta > 0$. In such a siphon valve (Figure 6, middle), the meniscus stops at a first equilibrium position r_1 in the inbound section with a negative offset $\Delta r < 0$, i.e., $r_1 < r_0$. This distribution leads to a retention rate

$$\Omega_{\mathrm{cps}} = \sqrt{\frac{4\sigma \cos\Theta}{\varrho \cdot \bar{r}\Delta r \cdot D}} \tag{19}$$

(neglecting the capillary pressure at the meniscus in the large inlet reservoir) which results in $\Omega_{\mathrm{cps}}/2\pi \approx 10\ \mathrm{Hz}$ and $16\ \mathrm{Hz}$ for water under typical conditions, and $\Theta = 70°$ and $0°$, respectively; any spin frequency $\omega > \Omega_{\mathrm{cps}}$ will retain the liquid.

The second equilibrium position is reached at $\omega = \Omega^*_{\mathrm{cps}}$ with the meniscus at $r_2 > R_{\mathrm{crest}}$ in the outlet segment. Any further progression $r > r_2$ of the meniscus will then grow Δr to establish $p_\omega + p_\Theta > 0$, and thus trigger continuous siphoning.

As a low-pass valve, capillary primed siphons are particularly suitable for LUOs requiring strong centrifugal fields f_ω (1). The spread $\Delta\Omega_{\mathrm{cps}}$ of the threshold frequency Ω_{cps} (12), which might be related to poor definition of the contact angle Θ, is normally less practical relevance, as long as Θ stays sufficiently below 90°

In purely capillary-driven priming at $\omega = 0$, the time

$$T_\Theta = \frac{4\eta \cdot l^2}{D \cdot \sigma \cos\Theta} \tag{20}$$

for covering the axial distance $l \approx L + Z + L_{\mathrm{crest}} + (R_{\mathrm{cham}} - R_{\mathrm{crest}})$ scales with l^2, the viscosity of the liquid η, and inversely with its surface tension σ and $\cos\Theta$, and the cross-sectional diameter of the channel D.

Lost Volume

Transfer by centrifugal siphoning (Figure 6) often leaves a certain fraction $U_{\mathrm{loss}} < U_0 + \mathrm{U}_\Delta$ of the original liquid volume U_0 behind (Figure 8). The separation of this residual volume occurs when air is drawn into filled outlet channel during forward pumping, so the initially coherent liquid plug acting as "pulley" tears apart (Figure 8a). This residual volume ideally vanishes $U_{\mathrm{loss}}/U_0 \ll 1$, or exhibits a small spread $\Delta U_{\mathrm{loss}}/U_{\mathrm{loss}} \ll 1$; however, in practice, U_{loss} and ΔU_{loss} sensitively depend on the hydrodynamics and shape of Γ, and tend to decrease with the cross section A. Overflow driven liquid transfer running without a pulley mechanism (Figure 8b) tend to reduce the spread ΔU_{loss}, while producing larger absolute losses U_{loss}.

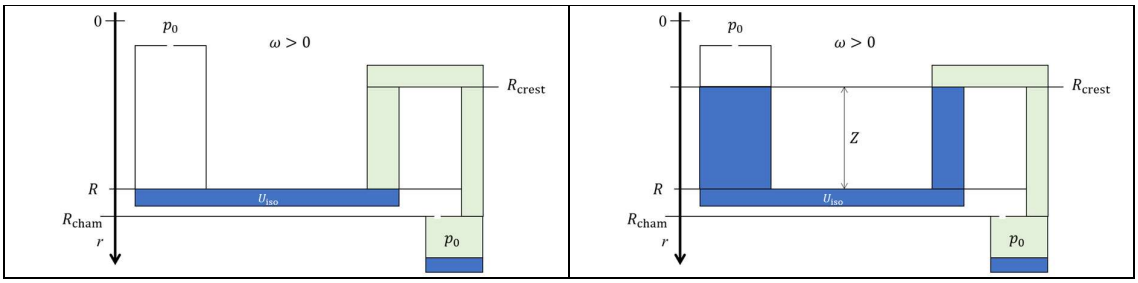

Preprints (www.preprints.org) | NOT PEER-REVIEWED | Posted: 27 May 2021 doi:10.20944/preprints202105.0683.v1

(a) Liquid $U_{\mathrm{loss}} \approx U_{\mathrm{iso}}$ residing in siphon structure Γ after "pulley" type siphoning failed to empty the isoradial channel of volume U_{iso}. This volume U_{loss} detaches from the liquid as air in sucked into the liquid plug.	(b) Liquid volume $U_{\mathrm{loss}} = U_{\mathrm{iso}} + (A_0 + A) \cdot Z$ remaining in Γ with pure overflow driven siphoning, which is favored for larger cross sections A of of the radially outbound channel, for which the liquid just "drizzels" out after passing the crest point.

Figure 8 Residual volume in centrifugal siphoning. After the transfer, part of the liquid U_0 is left in the siphon structure. U_{loss} sensitively depends on the shape of critical parts of Γ; it would ideally be 0, or at least reproducible, i.e., $\Delta U_{\mathrm{loss}} \approx 0$.

Centrifugo-Pneumatic Dissolvable-Film Siphon Valving

The geometry Γ in Figure 9 constitutes a hybrid of centrifugo-pneumatic (CP) valves (Figure 3), sacrificial dissolvable-film (DF) barriers (Figure 5) and centrifugal siphoning (Figure 6). Its transition between the two hydrostatic equilibrium distributions $\Lambda_{i\in\{1,2\}}$ results from a centrifugally induced pumping pressure p_ω (3) running against a pneumatic back pressure $p_z = p_{\leftarrow} = p_V$ (9). This configuration thus obviates the need for priming by interim addition V_Δ (Figure 6, top), hard to manufacture circumferential hydrophilic coating $\Theta < 90°$ of the narrow outlet channel (Figure 6, middle) and difficult to control pneumatic charging of a side chamber (Figure 7). Liquid transfer relies on volume overflow through channel segments with sufficiently large cross sections A.

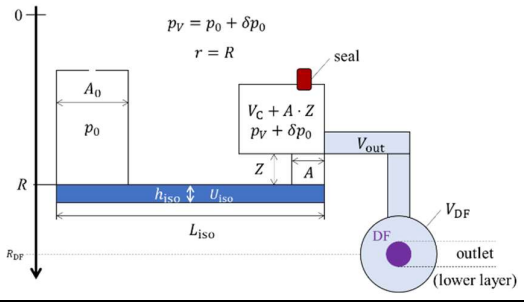

(a) Loading of isoradial segment with U_{iso} at $\omega = 0$ so a gas volume $V_{\mathrm{C}} + A \cdot Z$ is enslosed at a pressure $p_0 + \delta p = p_0 \cdot (1 + \chi)$ with respect to the atmosphere at p_0 and $\chi \ll 1$ representing pontential priming effects.

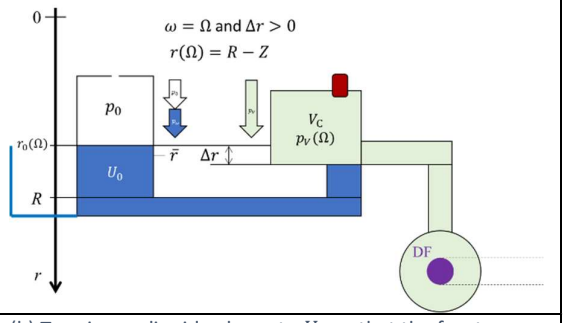

(b) Topping up liquid volume to U_0 so that the front meniscus settles at $r = R - Z$ when spinning at the (maximum) retention rate $\omega = \Omega$.

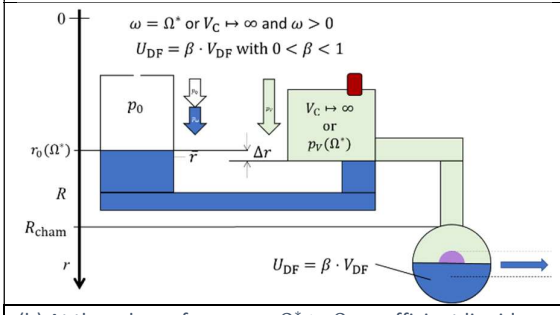

(b) At the release frequency $\Omega^* > \Omega$, a sufficient liquid volume $U_{\mathrm{DF}} = \beta \cdot V_{\mathrm{DF}}$ corresponding to a fraction $0 < \beta < 1$ of the dead volume V_{DF} of the outer chamber has overflown to open the DF.

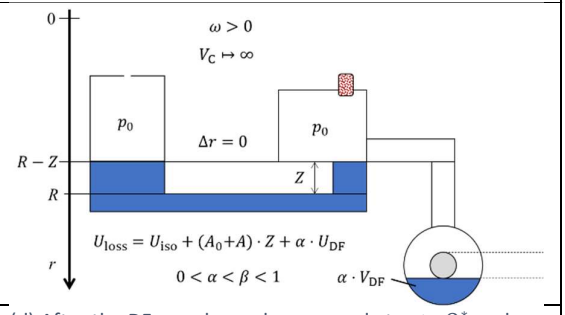

(d) After the DF membrane has opened at $\omega > \Omega^*$, or by venting $V_{\mathrm{C}} \mapsto \infty$, the liquid underneath the crest point $r \geq R - Z$ and $\alpha \cdot V_{\mathrm{DF}}$ with $0 < \alpha < \beta$ remains in Γ.

Figure 9 Operational principle of the siphon-shaped CP-DF siphon valve (not to scale).

During retention of this high-pass siphon valve $\omega < \Omega$, the meniscus stabilizes in the radially inbound section of the siphon channel, thus effectively dampening inertial overshoot by p_m (8) at finite flow rates $Q > 0$, suppressing premature droplet break-off of CP valves (Figure 3) and radial squeezing the meniscus for alternative layouts with isoradially directed outlets (Figure 2, right & Figure 3,

Preprints (www.preprints.org) | NOT PEER-REVIEWED | Posted: 27 May 2021 doi:10.20944/preprints202105.0683.v1

right). Even without direct experimental data, the better overall management of loading U_0 with smaller and more reproducible pressure offset δp_0 than for the basic CP-DF valve (Figure 3). The DF initially sealing the final pneumatic chamber allows rotationally controlled opening without external actuators as well as venting mode, while also removing the end-point character of the receiving chamber.

For these multiple, synergistical benefits, we consider CP-DF siphon valves as a key enabler for microfluidic larger-scale integration (LSI) at high operational reliability, and thus designate a separate section for them. For sake of clarity, we use a simplified geometry Γ to represent the valving structures and the resulting, quasi static liquid distributions Λ that lend themselves to description by analytical formulas, rather than the previous integrals. The basic concept has been outlined and experimentally validated in prior publications [61, 62, 80, 81].

Functional Principle

Loading

To best illustrate the basic principle of the CP-DF siphon valving, a (hypothetical) multi-step loading procedure is portrayed in Figure 9. At rest $\omega = 0$, a liquid volume U_{iso} completely fills the isoradial section of radial position R, length L and height h. This way, a pneumatically isolated gas pocket occupies a volume $V_{\mathrm{C}} + A \cdot Z$. The product $A \cdot Z$ represents the volume of the inbound siphon segment of cross section A and length Z, while V_{C} is mainly composed of the volume of the large chamber at its inner end, the segmented internal channel V_{int}, and the final recess chamber volume V_{DF} positioned at R_{cham}, i.e., typically $V_{\mathrm{int}} + V_{\mathrm{DF}} \ll V_{\mathrm{C}}$. The pressure in this gas pocket corresponds to $p_0 + \delta p_0 = p_0 \cdot (1 + \chi)$ with $0 \leq \chi \ll 1$ and the ambient pressure p_0 applying to the open inlet.

The total liquid volume is then topped up to $U_0 = U_{\mathrm{iso}} + A_0 \cdot [R - r_0(\Omega)] + A \cdot [R - Z]$, so that at the retention spin rate $\omega = \Omega$, the liquid distribution $\Lambda(\Omega)$ places its front meniscus at $r_1(\Omega) = R - Z$ (Figure 9b). For $\omega < \Omega$, we the front meniscus r_1 stays in the interval $R - Z < r_1(\omega) < R$.

Pneumatic Pressure

Due to the linked compression of the enclosed gas volume by $A \cdot (R - Z)$, the resulting increase in the pneumatic counterpressure

$$p_V(R, \Gamma, U_{\mathrm{DF}}, p_0, \chi, r) = p_{\leftarrow} = p_0 \cdot (1 + \chi) \cdot \left(\frac{V_{\mathrm{C}} + A \cdot Z}{V_{\mathrm{C}} + A \cdot [Z - (R - r)] - U_{\mathrm{DF}}} \right) \tag{21}$$

can thus be expressed by r with the liquid volume in the DF chamber U_{DF} vanishing during retention at $\omega \leq \Omega$.

Meniscus Position

Considering that the inner meniscus position in the inlet reservoir

$$r_0[R, \Gamma, U_0, U_{\mathrm{DF}}, r(\omega)] = R - \frac{U_0 - U_{\mathrm{iso}} - A \cdot [R - r(\omega)] - U_{\mathrm{DF}}}{A_0} \tag{22}$$

is a linear in r, the radial product $\bar{r}\Delta r$ in (4) and thus also the driving pressure $p_\omega \propto \bar{r}\Delta r$ (3) are square functions in r. With $p_{\rightarrow} = p_0 = \mathrm{const.}$, the hydrostatic equilibrium for the CP-DF siphon valves $p_\omega + p_0 = p_V$ (9) can be written as a cubic function in r. Thus, analytical solutions $r = r(R, \Gamma, U_0, U_{\mathrm{DF}}, p_0, \chi, \omega)$ can be found for a given geometry of the CP-DF siphon valve $\Gamma = \Gamma(A_0, A, U_{\mathrm{iso}})$ which are parametrized by common experimental parameters, such as the spin rate ω, the radial position R, the compression volume V_{C} and the loaded liquid volume U_0.

Preprints (www.preprints.org) | NOT PEER-REVIEWED | Posted: 27 May 2021 doi:10.20944/preprints202105.0683.v1

Liquid Retention

Critical Spin Rate

When the Λ assumes $r_1 = R - Z$ of its front meniscus at the upper end of the inbound segment (Figure 9a), inserting p_V (21) into (10) provides

$$\Omega(R, \Gamma, U_0, \chi) = \sqrt{\frac{p_0 \cdot \left[(1+\chi) \cdot \frac{V_C + A \cdot Z}{V_C} - 1\right]}{\varrho \cdot \bar{r}\Delta r}} \approx \sqrt{\frac{p_0}{\varrho \cdot \bar{r}\Delta r} \cdot \frac{A \cdot Z}{V_C}} \tag{23}$$

for the critical retention rate Ω for the CP-DF siphon valve.

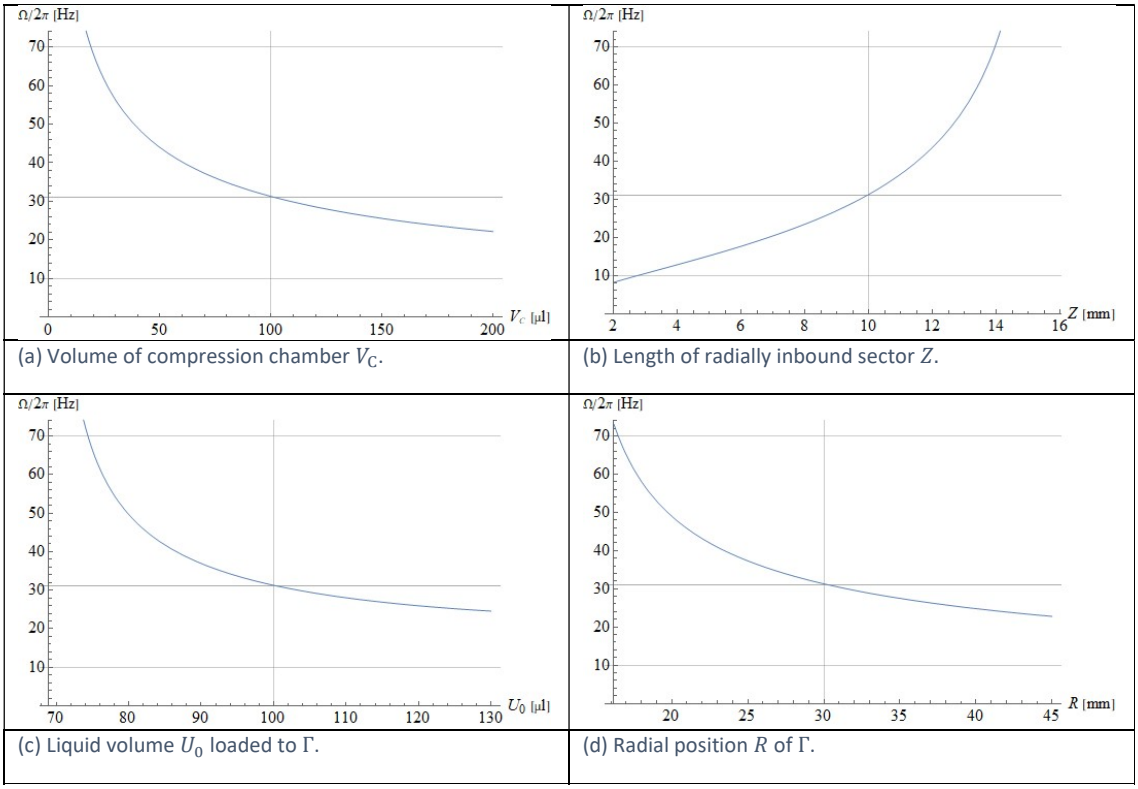

(a) Volume of compression chamber V_C.

(b) Length of radially inbound sector Z.

(c) Liquid volume U_0 loaded to Γ.

(d) Radial position R of Γ.

Figure 10 Critical spin frequency $\Omega/2\pi$ as a function of individual experimental input parameters (for $\chi \ll 1$). According to (23), Ω depends on (a) the compression volume V_C, i.e., $\Omega \propto 1/\sqrt{V_C}$. As for a given U_0, Δr rapidly shrinks with growing Z, while less affecting $\bar{r}$, Ω increases steeply towards large Z (b). For $r_1(\Omega) = R - Z$, enlarging the volume U_0 lets Δr grow faster than $\bar{r}$ decreases, so the retention rate Ω lowers with U_0 (c) and the radial position R (d).

Figure 10 examines the dependence of the critical spin rate Ω on select dimensions of the valve geometry Γ (top row), and the loaded liquid volume U_0 and radial position R (bottom row). The retention rate Ω is highly configurable, reducing with increasing volume V_C of the permanently gas-filled compression chamber (Figure 10a). Ω also grows by extending the length of the radially inbound segment Z (Figure 10b). As r_0 is linear in R and U_0 (22), the radial product $\bar{r}\Delta r$ is a square function in r_0, so Ω decreases with U_0 (Figure 10c) and R (Figure 10d), roughly following $1/U_0$ and $1/R$, respectively.

Tuning of Critical Spin Rate

As $r_0(\Omega)$ (22) in linear in U_0/A_0, also the radial product $\bar{r}\Delta r$ (4) and thus Ω (23) remain unaltered for $U_0/A_0 = \text{const}$. Hence, an LUO requiring retention of a different liquid volume U_0 keeps the same critical spin rate Ω (23) as long as the cross section of the inlet A_0 is adjusted by the same factor.

Preprints (www.preprints.org) | NOT PEER-REVIEWED | Posted: 27 May 2021 doi:10.20944/preprints202105.0683.v1

Figure 10 also reveals that the retention rate Ω (23) may be tuned in the range $10\ \mathrm{Hz} < \Omega/2\pi < 70\ \mathrm{Hz}$. Considering the effort to optimise manufacture processes to a specific design, it is usually wise to leave the essential, liquid carrying parts of Γ unaltered when adjusting the critical spin rate Ω (23) to the requirements of the assay protocol. Therefore, tuning of Ω (23) is preferentially implemented by rather large volume of the compression chamber V_C while maintaining the main part of Γ. In situations when the radial position R needs to be shifted, e.g., through space requirement, the relation (23) provides a recipe to compensate the shift in R by adjusting V_C.

Note that the permanently gas-filled sections only contribute with their total (dead) volume V_C to Ω (23), but they can be partitioned, distributed and located anywhere as long as being in pneumatic communication with each other. For instance, the compression volume V_C might be constituted by a smaller "attachment" to the inner end of the radially inbound section which is connected through a channel of tiny cross section to a larger chamber placed where space would be available in a multiplexed (disc) layout (see also the advanced geometry in the supplementary Figure S1).

Liquid Release

Modes

The considerations have so far focussed on the barrier function of CP-DF valving for$0 < R - r < Z$ by keeping $\omega < \Omega$. The opening condition is captured by the overflow of a minimum volume $U_\mathrm{DF} = \beta \cdot V_\mathrm{DF}$ with $0 < \beta < 1$ to sufficiently wet and disintegrate the DF, thus opening and venting the outer chamber of total volume V_DF; in Figure 9c, $\beta = 0.5$ for a central location in a recess with round cross section. After opening the DF at $\omega > \Omega^* > \Omega$ (Figure 9, bottom, left), or by perforation of a seal (Figure 9c), the compression compartment is vented, i.e., $V_\mathrm{C} \mapsto \infty$ and $p_V \mapsto p_0$, and any spin rate $\omega > 0$ will propel further liquid transfer (Figure 9, bottom, right). On the analogy of Figure 5, an additional seal or the DF might be opened by an external actuator [48, 82], or by a preceding liquid handling step, e.g., through "event-triggering" [62].

This transfer of $U_\mathrm{DF} = \beta \cdot V_\mathrm{DF}$ into the recess reduces the original liquid and gas volumes U_0 and $V_\mathrm{C} + A \cdot Z$, respectively, by U_DF, while the forward meniscus remains pinned to $r_1 = R - Z$. We calculate the release rate

$$\Omega^* = \sqrt{\frac{1}{\varrho \bar{r} \Delta r (U_0 - \beta \cdot V_\mathrm{DF})} \cdot p_0 \cdot \left[(1 + \chi) \cdot \frac{V_\mathrm{C} + A \cdot Z}{V_\mathrm{C} - \beta \cdot V_\mathrm{DF}} - 1 \right]} \qquad (24)$$

from (23) by considering the cutback of the loaded volume U_0 upstream of the crest point and the compression volume by $U_\mathrm{DF} = \beta \cdot V_\mathrm{DF}$ in $\bar{r}\Delta r$ and p_V (5), respectively. These reductions result in a defined increment of the spin rate $\Omega_\mathrm{step} = \Omega^* - \Omega$ which grows with U_DF. The gap Ω_step can thus be tuned for CP-DF siphon valves through Γ, for instance, by dead volume of the outer chamber outside $r \geq R_\mathrm{DF}$. For common CP-DF siphon valves, $\beta \cdot V_\mathrm{DF}/V_\mathrm{C} \ll 1$, so that the $0 < \Omega_\mathrm{step}/\Omega \ll 1$.

The opening mechanism of the CP-DF siphon valve (Figure 9) imposes the general volume condition $A_0 \cdot [R - Z - r_0(\Omega^*)] \geq U_\mathrm{DF}$ for both, actuation by rotation or venting, to assure $\Delta r > 0$, and thus a non-vanishing centrifugal field $p_\omega \propto \Delta r$, to drive liquid transfer through the outlet for any $\omega > 0$ subsequent to the removal of the DF or seal of the compression chamber. Note that strictly speaking, $\omega < \Omega$ describes "clean" retention without overflow into the DF chamber while, in principle, $\omega < \Omega^*$ would be sufficient. Yet, for practical reasons, it is turns out best to avoid overflow into the DF chamber during retention phase.

Preprints (www.preprints.org) | NOT PEER-REVIEWED | Posted: 27 May 2021 doi:10.20944/preprints202105.0683.v1

Reliability

Consistent valving requires that the forward meniscus needs to stay at $r(\omega = \Omega - M \cdot \Delta\Omega) > R - Z$ during retention; for reliable rotational actuation, $\omega \geq \Omega^* + M \cdot \Delta\Omega^*$. Beyond the factors impacting $\Delta\Omega$, the uncertainty $\Delta\Omega_{\mathrm{step}}$ is thus mainly determined by the definition of the volume fraction $\beta \cdot V_{\mathrm{DF}}$. For typical experimental conditions $\Omega_{\mathrm{step}}/\Omega \ll 1$, robust rotational actuation thus comes down to $\omega \geq \Omega^* + M \cdot \Delta\Omega^* \approx \Omega + M \cdot \Delta\Omega$, so that a "forbidden" frequency band of width $2 \cdot M \cdot \Delta\Omega$ around $\omega = \Omega$ must be crossed for reliable switching the CP-DF siphon valve (see also Figure 1).

Residual Volume

As already investigated in the context of basic siphon valving (Figure 8), the accuracy and precision of the transferred liquid volume directly enters mixing ratios underpinning bioanalytical quantitation, and also the Ω (23) and Ω^* (24) for subsequent valving steps, and thus critically impacts system level reliability of microfluidic LSI.

Neglecting inertial and interfacial effects, pure $\Delta r > 0$ driven overflow across the crest channel, and a fraction $\alpha \cdot V_{\mathrm{DF}}$ with $0 < \alpha < \beta < 1$ remaining in the recess for the DF, the volume

$$U_{\mathrm{loss}} = (A_0 + A) \cdot Z + U_{\mathrm{iso}} + \alpha \cdot V_{\mathrm{DF}} \tag{25}$$

constitutes an (approximate) upper boundary of liquid lost after the transfer (Figure 9d). U_{loss} (25) displays direct contribution of U_{iso} and increases linearly with Z as well as the cross sections A_0 and A. Note that especially for the here assumed, sufficiently large cross section A, "pulley"-type siphoning is absent, thus optimizing volume definition by minimizing ΔU_{loss}, which might be further improved via proper definition of a "cut-off" by placing a sharp-edged "liquid knife" within a low dead-volume section.

Rotational Valving Schemes

The objective of the digital twin concept presented here is to support the choice and layout of rotationally controlled valving techniques at the pivot of LoaD systems featuring high functional integration density with "*in silico*" predictable, system-level reliability for rapid and cost-efficient scale-up of manufacture from prototyping (for initial fluidic testing) to pilot series (for initial bioanalytical testing) and commercial mass fabrication. This section proposes a repertoire of metrics quantifying key performance indicators (KPIs) which help the selection of the type and layout of rotationally controlled valving for a given scenario.

Performance Metrics

Critical Frequencies and Field Strengths

For a given high-pass valve, maximum field strengths $f_\omega(\widehat{\Omega}) \propto \widehat{\Omega}^2\sqrt{\Delta r}$ for capillary burst (12)

$$f_\Theta \approx \varrho \cdot \bar{r} \cdot \Omega_\Theta^2 \approx \frac{4\sigma}{\Delta r}\frac{(-\cos\Theta)}{D} \tag{26}$$

and basic CP valves (16)

$$f_{\mathrm{CP}} \approx \varrho \cdot \bar{r} \cdot \Omega^2 \approx \frac{p_0}{\Delta r} \cdot \frac{A \cdot Z}{V_{\mathrm{C}}} \tag{27}$$

as well as for the CP-DF siphoning structure (23) of retention rate $\widehat{\Omega}$ cannot be exceeded during processing an upstream LUO. For the low-pass mechanisms, there is, *per definitionem*, only a critical

Preprints (www.preprints.org) | NOT PEER-REVIEWED | Posted: 27 May 2021 doi:10.20944/preprints202105.0683.v1

rate $\breve{\Omega}$ for valve opening at $\omega < \breve{\Omega}$. For the capillary primed siphon (Figure 6b), there is a minimum field strength

$$f_{\mathrm{cps}} \approx \varrho \cdot \bar{r} \cdot \Omega_{\mathrm{cps}}^2 \approx \frac{4\sigma \cos\Theta}{\Delta r \cdot D} \tag{28}$$

which will have to be calculated numerically for the pneumatic priming (Figure 7). In most LUOs, such a minimum field strength f is not relevant in the vast majority of applications.

For the CP valves (for $\chi = 0$), we find, by revisiting at (16) and (23), that the difference $p_{\leftarrow} - p_{\rightarrow}$ becomes $p_0 \cdot A \cdot Z/V_{\mathrm{C}}$, so $\widehat{\Omega} \propto \sqrt{A \cdot Z/V_{\mathrm{C}}}$. Mathematically, its scaling with $1/\sqrt{V_{\mathrm{C}}}$ allows to raise the retention rate $\widehat{\Omega}$ to any required value by downsizing the compression volume V_{C}. The same holds for capillary burst valves with $p_{\leftarrow} = p_{\Theta} \propto \sigma \cdot \cos\Theta/D$ (6) with vanishing $p_{\rightarrow} \approx 0$ when lowering the diameter of the constriction D. However, in practice, shrinking V_{C} and D is limited by the minimum feature sizes of the manufacturing technologies (and growing spread $\Delta\Omega$), and also the product $\sigma \cdot \cos\Theta$ has upper limits for capillary valves.

Apart from its linearity in $\sqrt{p_{\leftarrow} - p_{\rightarrow}}$, we also observe that the retention rate $\widehat{\Omega} \propto 1/\sqrt{\bar{r}\Delta r}$ (10) can be increased by minimizing the geometrical product $\bar{r}\Delta r$ representing the radial coordinates of the liquid distribution Λ within the valving structure Γ. This dependence unravels a clear advantage of siphoning strategies where the Δr and $\bar{r}$ only refer to the radial distribution of Λ between the menisci r_0 and r in the inlet and inbound section, respectively, while the outer volumes extending between r and R plus U_{iso} do not enter $\widehat{\Omega}$ (10), and can thus be "randomly" large.

So, in contrast to the basic capillary (Figure 2) or CP (Figure 3) modes where $\Delta r = R + Z - r_0$ and $\bar{r} = 0.5 \cdot (R + Z + r_0)$ hold during retention, siphon valving can be geared for high retention rates $\widehat{\Omega}$ (10) by "hiding" the bulk liquid volume outside r, while minimizing the radial extension Δr and / or the mean position $\bar{r}$ of the inner liquid distribution Λ in the radial interval between r_0 and r. Note, however, that maximization of $\Omega \propto 1/\sqrt{\Delta r}$ hits a limit as the volume $A_0 \cdot \Delta r$ has to be sufficient to effectuate complete filling of the channel section extending between the position r_1 during retention to r_2 for triggering liquid release.

Band Width

The metric

$$\overline{\Delta\Omega} = \frac{\Delta\Omega}{\omega_{\mathrm{max}} - \omega_{\mathrm{min}}} \tag{29}$$

reflects the statistical spread of the critical frequency Ω to variations in the experimental input parameters with respect to the practically available spin rate corridor between ω_{min} and ω_{max}. Minimisation of $\overline{\Delta\Omega}$ (29) can thus guide the development of tolerance-forgiving designs.

For rotationally actuated siphon valving (Figure 6), the retention and release frequencies Ω and release Ω^* can be tuned separately. Both spin rates need to be sufficiently spaced to account for their individual spreads $\Delta\Omega$ and $\Delta\Omega^*$, in addition the differential in the spin rate ω to lift the meniscus to a target location past the second (unstable) equilibrium distribution Λ to r_2 located past the crest point at R_{crest}, or even further to deliver a minimum liquid volume U_{DF} to the outer chamber for ushering CP-DF siphon valving (Figure 9). This requires reserving a band $\Omega - M \cdot \Delta\Omega < \omega < \Omega^* + M \cdot \Delta\Omega^*$ for the spin rate ω. Towards LSI, it is thus favourable to minimise the metric

$$\overline{\Delta\Omega^*} = \frac{(\Omega^* + M \cdot \Delta\Omega^*) - (\Omega - M \cdot \Delta\Omega)}{\omega_{\mathrm{max}} - \omega_{\mathrm{min}}} \tag{30}$$

Preprints (www.preprints.org) | NOT PEER-REVIEWED | Posted: 27 May 2021 doi:10.20944/preprints202105.0683.v1

in order to be able to “squeeze” as many fluidic operations as possible into the available frequency range.

Volume Loss

Upon completion of valving, a part $U_{\mathrm{loss}} = \zeta \cdot U_0$ with $0 \leq \zeta < 1$ of the originally loaded volume U_0 might remain in the structure Γ (Figure 8). While $\zeta \mapsto 0$ for the basic radial valve setups (Figure 2 and Figure 3), the emptying of the siphon structures (Figure 6) runs against the centrifugal pressure head p_ω (3) in the inbound section once gas has compromised the integrity of the liquid plug to create a segment characterized by $\Delta r < 0$.

As sketched in Figure 9, siphon valving may be entailed by a loss of liquid volume U_{loss}, which is approximated for CP-DF valving by (25). In some bioassays, a systematic loss can be factored in by loading more liquid volume U_0 to the inlet. Still, accommodating U_{loss} (25) tends increase the footprint of liquid handling structures, critically enters the output volume $U_0 - U_{\mathrm{loss}}$, and thus the frequencies Ω (23) and Ω^* (24) of the subsequent valving step in LSI. A metric guiding design optimisation might thus be

$$\overline{U}_{\mathrm{loss}} = 1 - \frac{U_{\mathrm{loss}}}{U_0} \tag{31}$$

which converges towards unity when minimising U_{loss} (31).

Volume Precision

In the same way as the absolute amount of liquid determines the critical frequencies Ω (23) and Ω^* (24) of following flow control operations and concentrations, their statistical spreads ΔU_0 and ΔU_{loss} impact the precision of the inlet volume U_0 in the next step. While systematic losses may be factored into the design, stochastic fluctuations may even interrupt liquid handling sequences as the minimum amount of liquid needed to reach Ω^* (24) may not be available in the inlets of a subset of valves. We define the dimensionless ratio

$$\overline{\Delta U}_{\mathrm{loss}} = \frac{\Delta U_{\mathrm{loss}}}{U_{\mathrm{loss}}} \tag{32}$$

as the metric to be minimized for enhancing reliability of multiplexed valving.

Radial Extension

In multi-step assay protocols, the radial confinement of the disc between R_{min}, e.g., given by the size of an inner hole to clamp the disc to the spindle, and the largest radius R_{max} at which structures can still be placed, limits the number of LUOs that can be automated. A design goal may therefore be to radially compress each structure of radial extension ΔR_Γ of the LUO with its downstream control valve. ΔR_Γ will often correspond to the difference between the minimum radial position of the inner meniscus r_0 over the course of valving and the radially outer edge of the final receiving chamber. The metric

$$\overline{\Delta R} = \frac{\Delta R_\Gamma}{R_{\mathrm{max}} - R_{\mathrm{min}}} \tag{33}$$

might thus be chosen to guide optimisation of radial space for a rotationally valved LUO.

Real Estate

The total area available on the chip-based rotor given by $A_0 = \int_{R_{\mathrm{min}}}^{R_{\mathrm{max}}} 2\pi \cdot r dr = \pi(R_{\mathrm{max}}^2 - R_{\mathrm{min}}^2)$ is shared between LUOs and intermittent valves. Therefore, any space savings through clever valve design will enhance the potential for multiplexing. For establishing a metric of this footprint, we consider that the centrifugal field f_ω (1) is unidirectional, i.e., it cannot (directly) pump liquids

Preprints (www.preprints.org) | NOT PEER-REVIEWED | Posted: 27 May 2021 doi:10.20944/preprints202105.0683.v1

towards the centre of rotation; such centripetal pumping requires provision of power, e.g., connection of a pressure source [45], chemical reaction [73, 78] or imbibition [63, 83], or potential energy in the centrifugal field, e.g., through simultaneous displacement of a centrally stored (ancillary) liquids [84] or centrifugo-pneumatic siphoning [44]. The LUOs of assay protocols are therefore typically aligned in a radially increasing sequence along their order in their execution in the assay protocol. This also implies that the reservoirs taking up the sample and reagents to be processed may need to be located centrally.

Overall, these boundary conditions intrinsic to centrifugal microfluidic systems make central real estate more scarce and thus precious, which we reflect by the metric ("price tag")

$$\overline{A} = \frac{1}{R_{\max} - R_{\min}} \cdot \int_{R_{\min}}^{R_{\max}} \frac{W(r)}{2\pi r} dr \tag{34}$$

where $W(r)$ represents the total azimuthal width of the valve at a radial location r, e.g., the length of the isoradial channel L at $r = R$ in the simplified geometry of the CP-DF siphon valve (Figure 9). Note that for finite thickness of the fluidic substrate, typically on the order of millimeters, the area of liquid containing sectors of the CP-DF valve cannot be compressed arbitrarily compressed.

Valving Time

The interval between prompting the opening of a valve and the completion of the liquid transfer through its structure Γ to the subsequent stage involves different processes, which depend on the selected valving mechanism. For the core modes of hydrophobic barriers (Figure 2) and CP valving (Figure 3), the transfer time results from a centrifugally driven flow propelled by a pressure differential $p = p_\omega = \varrho \cdot \bar{r}\Delta r \cdot \Omega^2$ (3) through the radial outlet of length l and cross section A, resulting in a flow rate $Q \approx A^2/8\pi\eta \cdot p/l$ and transfer time

$$T_{\mathrm{Q}} \approx \frac{U_0}{Q} = \frac{8\pi\eta}{A^2} \cdot \frac{U_0 \cdot l}{\varrho \cdot \bar{r}\Delta r \cdot \Omega^2} \tag{35}$$

for the liquid of density ϱ and viscosity η. The approximation (35) neglects start up an exit effects when the channel is only partially filled, and assumes constant $\bar{r}\Delta r$ to provide a constant pumping pressure p. Of course, the product $\bar{r}(t)\Delta r(t)$ would develop over the course of transfer. As previously outlined, for siphon valving, $\bar{r}$ and Δr are calculated from r_0 and r, l refers to the aggregate axial length of the siphon and outlet channels, and Ω needs to be replaced by the release frequency Ω^* for rotational actuation modes.

By assuming typical values $U = 10\ \mu\mathrm{l}$, $A = (100\ \mu\mathrm{m})^2$, $l = 1\ \mathrm{cm}$, a mean radial position $\bar{r} = 3\ \mathrm{cm}$, $\Delta r = 1\ \mathrm{cm}$, $\Omega = 2\pi \cdot 25\ \mathrm{Hz}$ and the density $\varrho = 1000\ \mathrm{kg\ m^{-3}}$and viscosity $\eta \approx 1\ \mathrm{mPa\ s}$ roughly corresponding to water, we arrive at an order of magnitude for $T_Q \approx 3.4\ \mathrm{s}$ (35) for the basic radial valve configurations. When extending l by a factor of 5 reducing Δr by the same factor to account for siphoning, T_Q (35) increases by a factor of 25 to about $1.5\ \mathrm{min}$.

For release mechanisms implementing DFs, the dissolution time T_{DF} of the membrane adds to T_Q (35). T_{DF} can be set by the formulation and thickness of the film, and may require a minimum pressure $p_{\mathrm{DF}} \propto R_{\mathrm{DF}}$ on the film located at R_{DF} during wetting. Values for T_{DF} can range from seconds to minutes, and may display significant variation ΔT_{DF}. Note that various "timing" modules have been developed for LoaD systems , e.g., to delay or synchronize liquid handling with reaction periods [79] [63].

Preprints (www.preprints.org) | NOT PEER-REVIEWED | Posted: 27 May 2021 doi:10.20944/preprints202105.0683.v1

Configurability

The previous deliberations and formulas allowing to maintain or tune the retention, burst and release rates $\Omega = \Omega(R, \Gamma, U_0)$ and Ω^* and their associated band widths $\Delta\Omega$ and $\Delta\Omega^*$ of rotationally controlled valves through the shape and location R of Γ and U_0 play an important role. This digital twin will enable *in silico* simulation tools offering high predictive power for configuring designs which optimize functional integration, reliability and manufacturability. For CP-DF siphon valves (Figure 9), the far-ranging configurability of the retention rate Ω through the volume of the permanently gas filled compression chamber which can be located "anywhere" on the disc and "hiding" liquid volumes to reduce Δr by "hiding" liquid volume on the outer part of the structure Γ provides a major benefit (Figure 10).

Configurability might also play an important role in other, collective aspects of LSI, such as mechanical balancing of the disc (cavities), minimizing its moment of inertia $I_m = \frac{\pi}{2}\varrho_{\mathrm{disc}}R_0^4$, optimization of mould flow for its mass replication, and compatible interfacing with standard liquid handling robotics and workflows.

Comparison

Table 1 compiles the select metrics with their typical scaling behavior and value ranges for the previously outlined valving schemes. Note that, due to the plethora of parameters, their wide ranges, and refined designs, absolute assessments are impossible to make; the digital twin concept presented here will help to choose and improve the optimum valving concept for a given LoaD application.

Valving Principle	**Retention**	**Release**	**Retention: high ω**	**Band Width: low $\Delta\Omega$**	**Spatial Footprint**	**Configurability**	**Low U_{loss}**	**Low ΔU_{loss}**	**Transfer to next LUO**	**Manufacturability**
Hydrophobic constriction	$\omega \le \Omega_\Theta$ (12)	$\omega > \Omega_\Theta$ (12)	–	–	+	●	+	+	+	–
Centrifugo-pneumatic	$\omega \le \Omega_{\mathrm{cpv}}$ (14)	Rotational $\omega > \Omega_{\mathrm{cpv}}$ $\omega > \Omega_{\mathrm{cpv}}$ (16) $U_{\mathrm{DF}} > \beta \cdot V_{\mathrm{DF}}$	++	–	+	–	+	+	–	+
		Direct Venting $\omega > 0$ $V_{\mathrm{C}} \mapsto \infty$		+		+				–
Siphoning	$\Delta r(U_0) \le 0$	Volume priming $\Delta r(U_0 + U_\Delta) > 0$	++	++	●	++	–	++	+	++
	$\omega > \Omega_{\mathrm{pps}}$ (18)	Pneumatic priming $\omega < \Omega_{\mathrm{pps}}$ (18)		–	–	–	●	–		++
	$\omega > \Omega_{\mathrm{cps}}$ (19)	Capillary priming $\omega < \Omega_{\mathrm{cps}}$ (19)		–	●	●	+	–		–
CP-DF siphon valving	$\omega < \Omega$ (23) $U_{\mathrm{DF}} < \beta \cdot V_{\mathrm{DF}}$	Rotational $\omega > \Omega^*$ (24)	++	+	●	++	–	+	+	●
		Venting $V_{\mathrm{C}} \mapsto \infty$					●			–

Table 1 Overview of rotationally controlled valving schemes according to common assessment criteria. Each principle distinguishes by its retention and release mechanism. The columns provide criteria for benchmarking which depend on the

Preprints (www.preprints.org) | NOT PEER-REVIEWED | Posted: 27 May 2021 doi:10.20944/preprints202105.0683.v1

particular implementation, so their assessment indicates trends for typical implementations, i.e., R, Γ and U_0, rather than claiming absolute validity for all possibly configurations.

Summary & Outlook

Summary

We have surveyed basic, rotationally controlled valving techniques and modelled their critical spin rates Ω and other performance metrics as a function of their radial positions R, geometries Γ and loaded liquid volumes U_0. The underlying digital twin approach allows to efficiently select, configure and optimize the valve for typical design objectives, such as retention at high field strength during processing of a Laboratory Unit Operation (LUO) in the inlet reservoir, or to accommodate different reagent volumes U_0.

The modelling presented here specifically correlates retention rates Ω and their band widths $\Delta\Omega$ with experimental input parameters displaying statistical spreads resulting from pipetting, material properties, ambient conditions, and, in particular, the lateral and vertical precision of the manufacturing technique. This digital twin allows to engineer tolerance-forgiving valve designs displaying predictable functionality along scale-up from prototyping for demonstrating proof-of-concept to pilot series for extended bioanalytical testing and regulatory compliant mass manufacture.

Towards larger-scale integration (LSI) of fluidic function underpinning comprehensive sample-to-answer automation of multi-step / multi-reagent bioassay panels, the design-for-manufacture (DfM) capability of the digital twin thus allows maximizing the packing density in real and frequency space while assuring system-level reliability.

The high predictive power of the *in-silico* approach can thus substantially curb the risk, cost and time for iterative performance optimisation towards high technology readiness levels (TRLs), and thus efficiently supports systematic Failure Mode & Effects Analysis (FMEA), and advancement towards commercialisation. The general formalism developed for functional and spatial optimisation may well be adopted for other Lab-on-a-Chip platforms and applications.

Outlook

Several extensions of the rudimentary digital twin approach are proposed, e.g., in inclusion of previously introduced flow control by event-triggering, rotational pulsing and delay modules, or further increase of real estate by vertical stacking multiple fluidic layers. Valving performance can be improved by sophistication of valve layouts and migration from the hydrostatic model to computational fluidic dynamic (CFD) simulation. An advanced design tool could also include the bioassay kinetics. Virtual prototyping could also be extended by including the simulation of the manufacturing processes of the layouts themselves. This would be particularly suitable for more complex methods like mould flow for injection moulding or 3D printing.

Regarding the bigger picture, the ability to create larger-scale integrated, fluidically functional designs with predictable reliability may enable foundry models that are commonplace in mature industries such as microelectronics and micro-electro-mechanical systems (MEMS). These efforts might be supported by existing initiatives aiming at standardisation of interfaces, manufacture and testing [85-87]. As valving assumes a similar role on centrifugal LoaD platforms as transistors for the emergence of integrated circuits (ICs) in (digital) electronics, the community is well equipped with the presented digital twin approach to develop large-scale integrated “bioCPUs” – Centrifugal Processing Units for implementing comprehensive bioassay panels.

Preprints (www.preprints.org) | NOT PEER-REVIEWED | Posted: 27 May 2021 doi:10.20944/preprints202105.0683.v1

Follow-up work is already planned on computer-aided, possibly automated optimization of integration density, robustness and manufacturability. As open platform concept [88, 89], the work is meant to encourage further honing of design, modelling, simulation and experimental verification, for instance, within a blockchain-incentivized participatory research model involving crowdsourcing by means of hackathons, citizen science, fab / maker labs [90-92].

Supplementary Material

S1. Default Geometry

The structure Γ, loaded liquid volumes U_0 and radial positions R can be varied across a multi-dimensional parameter space, e.g., to tune retention rates Ω of other key performance indicators. Table S1 gives of overview or generic values which can be used to initiate optimization.

$R = 3$ cm	$R_{\min} = 1.5$ cm	$R_{\max} = 5.5$ cm	$R_{\mathrm{DF}} = 3.15$ cm $> R$
$A_0 = d_0 \cdot w_0$	$d_0 = 1$ mm	$w_0 = 5$ mm	
$U_0 = 100$ µl $< \mathrm{A}_0 \cdot (R - R_{\min})$			
$U_{\mathrm{iso}} = d_0 \cdot h \cdot L \ll U_0$	$d_{\mathrm{iso}} = 1$ mm	$h_{\mathrm{iso}} = 1$ mm	$L_{\mathrm{iso}} = 15$ mm $> w_0 + w$
$U_Z = d \cdot w \cdot Z$	$d = 500$ µm	$w = 800$ µm $\ll w_0$	$Z = 10$ mm
$V_{\mathrm{C}} = d_{\mathrm{C}} \cdot w_{\mathrm{C}} \cdot h_{\mathrm{C}} \gg U_Z$	$d_{\mathrm{C}} = 1$ mm	$w_{\mathrm{C}} = 10$ mm	$h_{\mathrm{C}} = 10$ mm
$V_{\mathrm{int}} = d_{\mathrm{int}} \cdot h_{\mathrm{int}} \cdot L_{\mathrm{int}} \ll V_{\mathrm{C}}$	$d_{\mathrm{int}} = 200$ µm	$h_{\mathrm{int}} = 300$ µm	$L_{\mathrm{int}} = 1$ cm $> 2w$
$V_{\mathrm{DF}} = 0.25\pi \cdot d_{\mathrm{DF}} \cdot D_{\mathrm{DF}}^2 \ll V_{\mathrm{C}}$	$d_{\mathrm{DF}} = 190$ µm	$D_{\mathrm{DF}} = 3$ mm	$\alpha = 0.45, \beta = 0.5$

Table S1 Default geometrical parameters and relationships of CP-DF siphon valves (Figure 9). The resulting critical spin rate $\Omega(R, \Gamma, U_0)/2\pi \approx 30$ Hz. Minimum lateral dimensions are given by the smallest practical diameter of milling tools (200 µm). As tools for injection molding are often adopted from optical data storage (e.g., CD, DVD, Blu-ray), a central, 1.5-cm diameter hole and a disc radius of 6 cm with thickness around 1.2 mm, fluidic structures Γ may need to stay within the radial interval between $R_{\min} = 1.5$ cm and $\mathrm{R}_{\max} = 5.5$ cm, and an upper limit for the depth of about 1 mm. The lowest depth of cavities is often restricted by the sealing technology; for large lateral extensions or small aspect ratios, sagging of the lid, which is often a foil, may significantly change the nominal volume capacity, also in response to the pressure, and might even lead to sticking to the bottom of the cavity.

S2. Consistency Checks

Not all *in silico* designed structures Γ turn out to provide proper valving with given volumes U_0 and critical spin rates Ω. One reason is manufacturability, the other fluidic function. Table S1 already introduces some rudimentary sanity checks as necessities, but not guaranteeing sufficiency for proper valving. As for other parts of this work, we exclude analysis of biochemical function, which may, for instance, be related to surface adsorption of (bio-)molecules in high surface-to-volume ratio channels, denaturing of biomolecules due to chemical agents leaching from bulk materials and assembly processes, viability of cells or reaction kinetics.

Fluidic Function

A common design goal is to set a certain retention and release rates Ω and Ω^* that are consistent with the valving sequence in frequency space for a liquid volume U_0 prescribed by the assay protocol. At least when discarding manufacturing restrictions, the basic radial layouts Γ displayed in Figure 2 and Figure 3 may be configured to any given critical frequencies Ω as long as the inlet reservoir can accommodate U_0, i.e., $U_0 < A_0 \cdot (R - R_{\min})$ for the hydrophobic barrier. Furthermore, the cross section of the outlet A needs to be sufficiently small to that surface tension maintains the integrity of the liquid plug.

However, proper functioning of the siphon-type valves (Figure 6) requires more complex design rules such as fundamental correlations between radial positions, linear dimensions and volumes are already included for (CP-DF) siphon valves. For example, to allow centrifugally energized outflow, the key radial positions of Γ need to be staggered according to $R_{\mathrm{crest}} < R < R_{\mathrm{out}}$ in order to transition

Preprints (www.preprints.org) | NOT PEER-REVIEWED | Posted: 27 May 2021 doi:10.20944/preprints202105.0683.v1

between the hydrostatic equilibria at $r_1 = r(\omega)$ and $r_2 = r(\Omega^*)$ in the inbound and outbound segments at $\omega = \Omega$ and Ω^*, respectively. So $R_{\text{crest}} < r_1 < R$ and $R_{\text{crest}} < r_2 < R_{\text{out}}$ needs to hold for the two targetted equilibrium positions of the front menisci. These conditions imply ranges $0 < U_0 - A_0 \cdot r_0(R, \Gamma, U_0, \Omega) - U_{\text{iso}} \leq A \cdot (R - R_{\text{crest}})$ and $0 < U_0 - A_0 \cdot r_0(R, \Gamma, U_0, \Omega^*) - U_{\text{iso}} - A \cdot Z - U_{\text{crest}} \leq A \cdot (R_{\text{out}} - R_{\text{crest}})$ for the loaded liquid volume U_0. In addition, the priming pressure $p_{\text{prime}} = p_\omega + p_\rightarrow - p_\leftarrow$ needs to stay positive along the entire, ω-controlled transition of high-pass ($\Omega < \omega < \Omega^*$) and low-pass ($\Omega^* < \omega < \Omega$) siphon valves of their front meniscus between its two equilibrium positions $r_1 = r(R, \Gamma, U_0, \Omega)$ to $r_2 = r(R, \Gamma, U_0, \Omega^*)$.

Manufacturability

The choice of the valving technology should also consider manufacturing aspects [93] of each scheme availed of during scale-up from prototyping to pilot series production and mass fabrication. While early centrifugal microfluidic platforms were often based on capillary pumping and valving, the local definition of contact angles Θ on all walls including the lid and its stabilization over time under different ambient conditions during storage, transport and deployment at the end user proves to be challenging. This work therefore emphasized valving schemes that would not require coating step during manufacture.

For each manufacturing technique, there are also technical and economical limitations regarding geometrical feature sizes and shapes, and their tolerances. For instance, minimum (lateral) dimensions of precision milling (of channels) are imposed by practicable tool diameters, in many cases about $200\ \mu\text{m}$, but rarely smaller than $100\ \mu\text{m}$; the tool radius furthermore determines the minimum curvature of (lateral) corners. As milling is a common way to prototype polymer LoaD substrates, and also for patterning replication tools, these restrictions apply to positive and negative structures of the original design. Note also that while milling offers a powerful structuring in a wide range of materials, machine times, tooling cost (and wear) and process development of subsequent replication can go rampant when increasing demands on specifications such as surface quality, optical finish, wobble, tool wear other deviations from “native” 2.5- to 3-dimensional geometries.

Especially for common polymer mass replication schemes like injection molding, a minimum wall thickness δW between all cavities needs to be observed. For instance, in the CP-DF siphoning valve in Figure 9, amongst the distances to be monitored are $Z > \delta W$ and $L = w_0 - w > \delta W$. Smooth demolding imposes upper limits on aspect ratios, and commonly requires the inclusion of draft angles, i.e., wall inclinations of the order of 5° to 15°. More complex criteria like an even distribution of the hydrodynamic resistance in the tool to avoid shadowing and inhomogeneous solidification during mould flow apply for the typically central, (compression-)injection of the hot melt need to be considered.

In addition to such “design-for-manufacture” (DfM) considerations of each scheme individually, it also needs to be observed that the technology along manufacturing scale-up might involve significantly diverging capabilities; therefore, the design restrictions introduced by the least capable scheme will have to be accounted for to assure seamless migration from prototyping to commercial production.

In particular tool making and optimization of mould flow are decisive cost drivers for microfluidic systems; layouts for new applications, i.e., centrifugally automated assay protocols, should ideally be derived, as much as possible, from designs that have already been previously validated while only varying parameters that are assumed to be less critical from fluidic, biological and manufacturing aspects.

Preprints (www.preprints.org) | NOT PEER-REVIEWED | Posted: 27 May 2021 doi:10.20944/preprints202105.0683.v1

S3. Advanced Design

In Figure S1, we fine-structure the original geometry for CP-DF siphoning of Figure 9; each compartment may have its specific depth, width and height to allow a wider space for multi-parameter optimization. Note that permanently gas-filled parts of the compression volume V_C may be moved to "any" location available in the disc as long as it is connected by a pneumatic interconnect to the DF chamber.

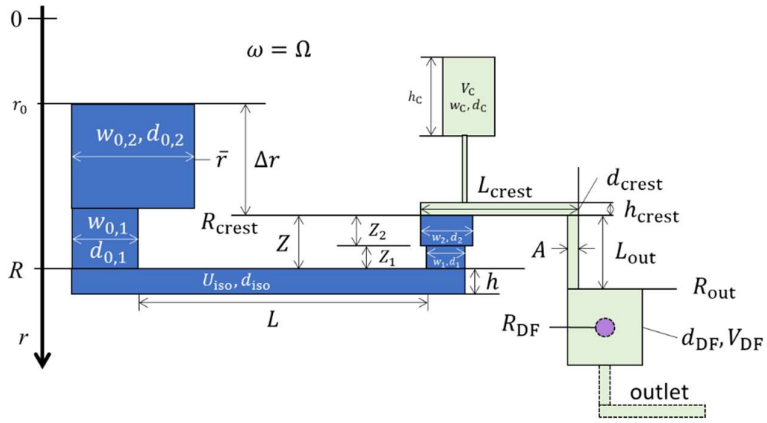

Figure S1 Advanced geometry with partitioned inlet reservoir and inbound segments, each having its individual depth, width, height and radial position for optimization of key performance indicators (KPIs). Note that any permanently gas filled part of the compression chamber can be randomly shaped and located "anywhere" on the disc (while still pneumatically to the liquid Λ).

Further variations might include inclination angles with respect to the radial and azimuthal directions, rounded shapes, branched structures to prevent blockage of air flow by residual liquid, liquid knifes for accurate metering of dispensed liquid volumes and draft angles for proper demoulding.

References

1. Manz, A., N. Graber, and H.M. Widmer *Miniaturized total chemical analysis systems: A novel concept for chemical sensing*. Sensors and Actuators B: Chemical, 1990. **1**, 244-248 DOI: 10.1016/0925-4005(90)80209-I.
2. Moore, G.E. *Cramming more components onto integrated circuits*. Electronics, 1965. **38**, DOI: 10.1109/N-SSC.2006.4785860.
3. Ducrée, J. *Efficient development of integrated Lab-On-A-Chip systems featuring operational robustness and nanufacturability*. Micromachines, 2019. **10**, 12 DOI: 10.3390/mi10120886.
4. Schembri, C.T., V. Ostoich, P.J. Lingane, T.L. Burd, and S.N. Buhl *Portable Simultaneous Multiple Analyte Whole-Blood Analyzer for Point-of-Care Testing*. Clinical Chemistry, 1992. **38**, 1665-1670 DOI: 10.1093/clinchem/38.9.1665.
5. Schembri, C.T., T.L. Burd, A.R. Kopfsill, L.R. Shea, and B. Braynin *Centrifugation and Capillarity Integrated into a Multiple Analyte Whole-Blood Analyzer*. Journal of Automatic Chemistry, 1995. **17**, 99-104 DOI: 10.1155/S1463924695000174.
6. *Abaxis*. Available on: https://www.abaxis.com/.

7. Andersson, P., G. Jesson, G. Kylberg, G. Ekstrand, and G. Thorsen *Parallel nanoliter microfluidic analysis system*. Analytical Chemistry, 2007. **79**, 4022-4030 DOI: 10.1021/ac061692y.
8. Inganas, M., H. Derand, A. Eckersten, G. Ekstrand, A.K. Honerud, G. Jesson, G. Thorsen, T. Soderman, and P. Andersson *Integrated microfluidic compact disc device with potential use in both centralized and point-of-care laboratory settings*. Clinical Chemistry, 2005. **51**, 1985-7 DOI: 10.1373/clinchem.2005.053181.
9. *Gyros Protein Technologies*. Available on: https://www.gyrosproteintechnologies.com/.
10. Madou, M.J. and G.J. Kellogg *The LabCD (TM): A centrifuge-based microfluidic platform for diagnostics*. Systems and Technologies for Clinical Diagnostics and Drug Discovery, Proceedings Of, 1998. **3259**, 80-93 DOI: 10.1117/12.307314.
11. Shea, M. *ADMET Assays on Tecan's LabCD-ADMET System*. Journal of the Association for Laboratory Automation, 2003. **8**, 74-77 DOI: 10.1016/s1535-5535(04)00260-6.
12. Smith, S., D. Mager, A. Perebikovsky, E. Shamloo, D. Kinahan, R. Mishra, S.M.T. Delgado, H. Kido, S. Saha, J. Ducrée, M. Madou, K. Land, and J.G. Korvink *CD-Based Microfluidics for Primary Care in Extreme Point-of-Care Settings*. Micromachines, 2016. **7**, DOI: 10.3390/mi7020022.
13. Kong, L.X., A. Perebikovsky, J. Moebius, L. Kulinsky, and M. Madou *Lab-on-a-CD: A Fully Integrated Molecular Diagnostic System*. Journal of the Association for Laboratory Automation, 2016. **21**, 323-355 DOI: 10.1177/2211068215588456.
14. Maguire, I., R. O'Kennedy, J. Ducrée, and F. Regan *A review of centrifugal microfluidics in environmental monitoring*. Analytical Methods, 2018. **10**, 1497-1515 DOI: 10.1039/c8ay00361k.
15. Gorkin, R., J. Park, J. Siegrist, M. Amasia, B.S. Lee, J.M. Park, J. Kim, H. Kim, M. Madou, and Y.K. Cho *Centrifugal microfluidics for biomedical applications*. Lab on a Chip, 2010. **10**, 1758-1773 DOI: 10.1039/b924109d.
16. Burger, R., L. Amato, and A. Boisen *Detection methods for centrifugal microfluidic platforms*. Biosensors and Bioelectronics, 2016. **76**, 54-67 DOI: 10.1016/j.bios.2015.06.075.
17. Mark, D., S. Haeberle, T. Metz, S. Lutz, J. Ducrée, R. Zengerle, and F. von Stetten *Aliquoting structure for centrifugal microfluidics based on a new pneumatic valve*. MEMS 2008: 21st Ieee International Conference on Micro Electro Mechanical Systems, Technical Digest, 2008. 611-+.
18. Schwemmer, F., T. Hutzenlaub, D. Buselmeier, N. Paust, F. von Stetten, D. Mark, R. Zengerle, and D. Kosse *Centrifugo-pneumatic multi-liquid aliquoting-parallel aliquoting and combination of multiple liquids in centrifugal microfluidics*. Lab on a Chip, 2015. **15**, 3250-3258 DOI: 10.1039/c5lc00513b.
19. Keller, M., S. Wadle, N. Paust, L. Dreesen, C. Nuese, O. Strohmeier, R. Zengerle, and F. von Stetten *Centrifugo-thermopneumatic fluid control for valving and*

aliquoting applied to multiplex real-time PCR on off-the-shelf centrifugal thermocycler. RSC Advances, 2015. **5**, 89603-89611 DOI: 10.1039/c5ra16095b.

20. Grumann, M., A. Geipel, L. Riegger, R. Zengerle, and J. Ducrée *Batch-mode mixing on centrifugal microfluidic platforms*. Lab on a Chip, 2005. **5**, 560-5 DOI: 10.1039/b418253g.
21. Ducrée, J., T. Brenner, S. Haeberle, T. Glatzel, and R. Zengerle *Multilamination of flows in planar networks of rotating microchannels*. Microfluidics and Nanofluidics, 2006. **2**, 78-84 DOI: 10.1007/s10404-005-0056-5.
22. Burger, R.K., David; Cayron, Hélène ; Reis, Nuno ; Garcia da Fonseca, João;Ducrée, Jens *Siphon-induced droplet break-off for enhanced mixing on a centrifugal platform*. Inventions, 2020. **5**, DOI: 10.3390/inventions5010001.
23. Ducrée, J., S. Haeberle, T. Brenner, T. Glatzel, and R. Zengerle *Patterning of flow and mixing in rotating radial microchannels*. Microfluidics and Nanofluidics, 2006. **2**, 97-105 DOI: 10.1007/s10404-005-0049-4.
24. Strohmeier, O., S. Keil, B. Kanat, P. Patel, M. Niedrig, M. Weidmann, F. Hufert, J. Drexler, R. Zengerle, and F. von Stetten *Automated nucleic acid extraction from whole blood, B. subtilis, E. coli, and Rift Valley fever virus on a centrifugal microfluidic LabDisk*. RSC Advances, 2015. **5**, 32144-32150 DOI: 10.1039/c5ra03399c.
25. Brassard, D., M. Geissler, M. Descarreaux, D. Tremblay, J. Daoud, L. Clime, M. Mounier, D. Charlebois, and T. Veres *Extraction of nucleic acids from blood: unveiling the potential of active pneumatic pumping in centrifugal microfluidics for integration and automation of sample preparation processes*. Lab on a Chip, 2019. **19**, 1941-1952 DOI: 10.1039/c9lc00276f.
26. Karle, M., J. Miwa, G. Roth, R. Zengerle, and F. von Stetten *A Novel Microfluidic Platform for Continuous DNA Extraction and Purification Using Laminar Flow Magnetophoresis*. IEEE 22nd International Conference on Micro Electro Mechanical Systems (MEMS 2009), 2009. 276-279 DOI: 10.1109/Memsys.2009.4805372.
27. Kido, H., M. Micic, D. Smith, J. Zoval, J. Norton, and M. Madou *A novel, compact disk-like centrifugal microfluidics system for cell lysis and sample homogenization*. Colloids and Surfaces B-Biointerfaces, 2007. **58**, 44-51 DOI: 10.1016/j.colsurfb.2007.03.015.
28. Brenner, T., S. Haeberle, R. Zengerle, and J. Ducree, *Continuous centrifugal separation of whole blood on a disk*, in *Micro Total Analysis Systems 2004, Vol 1*. 2005. p. 566-568
29. Steigert, J., T. Brenner, M. Grumann, L. Riegger, S. Lutz, R. Zengerle, and J. Ducrée *Integrated siphon-based metering and sedimentation of whole blood on a hydrophilic lab-on-a-disk*. Biomedical Microdevices, 2007. **9**, 675-679 DOI: 10.1007/s10544-007-9076-0.
30. Kinahan, D.J., S.M. Kearney, N.A. Kilcawley, P.L. Early, M.T. Glynn, and J. Ducrée *Density-Gradient Mediated Band Extraction of Leukocytes from Whole Blood*

Using Centrifugo-Pneumatic Siphon Valving on Centrifugal Microfluidic Discs. PLOS ONE, 2016. **11**, e0155545 DOI: 10.1371/journal.pone.0155545.

31. Dimov, N., J. Gaughran, D. Mc Auley, D. Boyle, D.J. Kinahan, and J. Ducrée, *Centrifugally Automated Solid-Phase Purification of RNA*, in *2014 IEEE 27th International Conference on Micro Electro Mechanical Systems (MEMS)*. 2014: Cancun, Mexico. p. 260-263 DOI: 10.1109/MEMSYS.2014.6765625.
32. Gaughran, J., D. Boyle, J. Murphy, R. Kelly, and J. Ducrée *Phase-selective graphene oxide membranes for advanced microfluidic flow control*. Microsystems and Nanoengineering, 2016. **2**, 16008 DOI: 10.1038/micronano.2016.8.
33. Haeberle, S., R. Zengerle, and J. Ducrée *Centrifugal generation and manipulation of droplet emulsions*. Microfluidics and Nanofluidics, 2007. **3**, 65-75 DOI: 10.1007/s10404-006-0106-7.
34. Schuler, F., F. Schwemmer, M. Trotter, S. Wadle, R. Zengerle, F. von Stetten, and N. Paust *Centrifugal step emulsification applied for absolute quantification of nucleic acids by digital droplet RPA*. Lab on a Chip, 2015. **15**, 2759-2766 DOI: 10.1039/c5lc00291e.
35. Schuler, F., M. Trotter, M. Geltman, F. Schwemmer, S. Wadle, E. Dominguez-Garrido, M. Lopez, C. Cervera-Acedo, P. Santibanez, F. von Stetten, R. Zengerle, and N. Paust *Digital droplet PCR on disk*. Lab on a Chip, 2016. **16**, 208-216 DOI: 10.1039/c5lc01068c.
36. Ducrée, J., S. Haeberle, S. Lutz, S. Pausch, F. von Stetten, and R. Zengerle *The centrifugal microfluidic Bio-Disk platform*. Journal of Micromechanics and Microengineering, 2007. **17**, S103-S115 DOI: 10.1088/0960-1317/17/7/S07.
37. Lutz, S., D. Mark, G. Roth, R. Zengerle, and F. von Stetten *Centrifugal Microfluidic Platforms for Molecular Diagnostics*. Clinical Chemistry and Laboratory Medicine, 2011. **49**, S608-S608.
38. Tang, M., G. Wang, S.-K. Kong, and H.-P. Ho *A Review of Biomedical Centrifugal Microfluidic Platforms*. Micromachines, 2016. **7**, DOI: 10.3390/mi7020026.
39. Duffy, D.C., H.L. Gillis, J. Lin, N.F. Sheppard, and G.J. Kellogg *Microfabricated Centrifugal Microfluidic Systems: Characterization and Multiple Enzymatic Assays*. Analytical Chemistry, 1999. **71**, 4669-4678 DOI: 10.1021/ac990682c.
40. Azimi-Boulali, J., M. Madadelahi, M.J. Madou, and S.O. Martinez-Chapa *Droplet and Particle Generation on Centrifugal Microfluidic Platforms: A Review*. Micromachines, 2020. **11**, DOI: 10.3390/mi11060603.
41. Tang, M., G. Wang, S.K. Kong, and H.P. Ho *A Review of Biomedical Centrifugal Microfluidic Platforms*. Micromachines, 2016. **7**, DOI: 10.3390/mi7020026.
42. Strohmeier, O., M. Keller, F. Schwemmer, S. Zehnle, D. Mark, F. von Stetten, R. Zengerle, and N. Paust *Centrifugal microfluidic platforms: advanced unit operations and applications*. Chemical Society Reviews, 2015. **44**, 6187-229 DOI: 10.1039/c4cs00371c.

43. Clime, L., J. Daoud, D. Brassard, L. Malic, M. Geissler, and T. Veres *Active pumping and control of flows in centrifugal microfluidics*. Microfluidics and Nanofluidics, 2019. **23**, DOI: 10.1007/s10404-019-2198-x.
44. Zehnle, S., F. Schwemmer, R. Bergmann, F. von Stetten, R. Zengerle, and N. Paust *Pneumatic siphon valving and switching in centrifugal microfluidics controlled by rotational frequency or rotational acceleration*. Microfluidics and Nanofluidics, 2015. **19**, 1259-1269 DOI: 10.1007/s10404-015-1634-9.
45. Clime, L., D. Brassard, M. Geissler, and T. Veres *Active pneumatic control of centrifugal microfluidic flows for lab-on-a-chip applications*. Lab on a Chip, 2015. **15**, 2400-2411 DOI: 10.1039/c4lc01490a.
46. Kinahan, D.J., M. Renou, D. Kurzbuch, N.A. Kilcawley, E. Bailey, M.T. Glynn, C. McDonagh, and J. Ducrée *Baking Powder Actuated Centrifugo-Pneumatic Valving for Automation of Multi-Step Bioassays*. Micromachines, 2016. **7**, DOI: 10.3390/mi7100175.
47. Mishra, R., J. Gaughran, D. Kinahan, and J. Ducrée *Functional Membranes for Enhanced Rotational Flow Control on Centrifugal Microfluidic Platforms*. Reference Module in Materials Science and Materials Engineering, 2017. DOI: 10.1016/b978-0-12-803581-8.04041-8.
48. Kinahan, D.J., P.L. Early, A. Vembadi, E. MacNamara, N.A. Kilcawley, T. Glennon, D. Diamond, D. Brabazon, and J. Ducrée *Xurography actuated valving for centrifugal flow control*. Lab on a Chip, 2016. **16**, 3454-3459 DOI: 10.1039/c6lc00568c.
49. *SpinX Technologies*. Available on: http://www.spinx-technologies.com.
50. Abi-Samra, K., R. Hanson, M. Madou, and R.A. Gorkin *Infrared controlled waxes for liquid handling and storage on a CD-microfluidic platform*. Lab on a Chip, 2011. **11**, 723-726 DOI: 10.1039/c0lc00160k.
51. Kong, L.X., K. Parate, K. Abi-Samra, and M. Madou *Multifunctional wax valves for liquid handling and incubation on a microfluidic CD*. Microfluidics and Nanofluidics, 2015. **18**, 1031-1037 DOI: 10.1007/s10404-014-1492-x.
52. Al-Faqheri, W., F. Ibrahim, T.H.G. Thio, J. Moebius, K. Joseph, H. Arof, and M. Madou *Vacuum/Compression Valving (VCV) Using Parrafin-Wax on a Centrifugal Microfluidic CD Platform*. PLOS ONE, 2013. **8**, DOI: 10.1371/journal.pone.0058523.
53. García-Cordero, J.L., F. Benito-Lopez, D. Diamond, J. Ducrée, and A.J. Ricco, *Low-Cost Microfluidic Single-Use Valves and on-Board Reagent Storage Using Laser-Printer Technology*, in *IEEE 22nd International Conference on Micro Electro Mechanical Systems (MEMS 2009)*. 2009: Sorrento, Italy. p. 439-442 DOI: 10.1109/Memsys.2009.4805413.
54. García-Cordero, J.L., D. Kurzbuch, F. Benito-Lopez, D. Diamond, L.P. Lee, and A.J. Ricco *Optically addressable single-use microfluidic valves by laser printer lithography*. Lab on a Chip, 2010. **10**, 2680-7 DOI: 10.1039/c004980h.
55. Torres Delgado, S.M., D.J. Kinahan, L.A. Nirupa Julius, A. Mallette, D.S. Ardila, R. Mishra, C.M. Miyazaki, J.G. Korvink, J. Ducrée, and D. Mager *Wirelessly*

powered and remotely controlled valve-array for highly multiplexed analytical assay automation on a centrifugal microfluidic platform. Biosensors and Bioelectronics, 2018. **109**, 214-223 DOI: 10.1016/j.bios.2018.03.012.

56. Park, J.M., Y.K. Cho, B.S. Lee, J.G. Lee, and C. Ko *Multifunctional microvalves control by optical illumination on nanoheaters and its application in centrifugal microfluidic devices*. Lab on a Chip, 2007. **7**, 557-64 DOI: 10.1039/b616112j.
57. Mishra, R., R. Alam, D.J. Kinahan, K. Anderson, and J. Ducrée, *Lipophilic-Membrane Based Routing for Centrifugal Automation of Heterogeneous Immunoassays*, in *2015 28th IEEE International Conference on Micro Electro Mechanical Systems (MEMS 2015)*. 2015: Estoril, Portugal. p. 523-526 DOI: 10.1109/MEMSYS.2015.7051007.
58. Godino, N., R. Gorkin, 3rd, A.V. Linares, R. Burger, and J. Ducrée *Comprehensive integration of homogeneous bioassays via centrifugo-pneumatic cascading*. Lab on a Chip, 2013. **13**, 685-94 DOI: 10.1039/c2lc40722a.
59. Zhao, Y., F. Schwemmer, S. Zehnle, F. von Stetten, R. Zengerle, and N. Paust *Centrifugo-pneumatic sedimentation, re-suspension and transport of microparticles*. Lab on a Chip, 2015. **15**, 4133-4137 DOI: 10.1039/c5lc00508f.
60. Henderson, B.D., D.J. Kinahan, J. Rio, R. Mishra, D. King, S.M. Torres-Delgado, D. Mager, J.G. Korvink, and J. Ducrée *Siphon-Controlled Automation on a Lab-on-a-Disc Using Event-Triggered Dissolvable Film Valves*. Biosensors, 2021. **11**, DOI: 10.3390/1108103.
61. Gorkin, R., 3rd, C.E. Nwankire, J. Gaughran, X. Zhang, G.G. Donohoe, M. Rook, R. O'Kennedy, and J. Ducrée *Centrifugo-pneumatic valving utilizing dissolvable films*. Lab on a Chip, 2012. **12**, 2894-902 DOI: 10.1039/c2lc20973j.
62. Kinahan, D.J., S.M. Kearney, N. Dimov, M.T. Glynn, and J. Ducrée *Event-triggered logical flow control for comprehensive process integration of multi-step assays on centrifugal microfluidic platforms*. Lab on a Chip, 2014. **14**, 2249-58 DOI: 10.1039/c4lc00380b.
63. Kinahan, D.J., S.M. Kearney, O.P. Faneuil, M.T. Glynn, N. Dimov, and J. Ducrée *Paper imbibition for timing of multi-step liquid handling protocols on event-triggered centrifugal microfluidic lab-on-a-disc platforms*. RSC Advances, 2015. **5**, 1818-1826 DOI: 10.1039/c4ra14887h.
64. Ducrée, J., S. Haeberle, S. Lutz, S. Pausch, F.v. Stetten, and R. Zengerle *The centrifugal microfluidic Bio-Disk platform*. Journal of Micromechanics and Microengineering, 2007. **17**, S103-S115 DOI: 10.1088/0960-1317/17/7/s07.
65. Brenner, T., T. Glatzel, R. Zengerle, and J. Ducrée *Frequency-dependent transversal flow control in centrifugal microfluidics*. Lab on a Chip, 2005. **5**, 146-50 DOI: 10.1039/b406699e.
66. Noroozi, Z., H. Kido, and M.J. Madou *Electrolysis-Induced Pneumatic Pressure for Control of Liquids in a Centrifugal System*. Journal of the Electrochemical Society, 2011. **158**, P130-P135 DOI: 10.1149/2.028111jes.

67. Abi-Samra, K., L. Clime, L. Kong, R. Gorkin, T.H. Kim, Y.K. Cho, and M. Madou *Thermo-pneumatic pumping in centrifugal microfluidic platforms*. Microfluidics and Nanofluidics, 2011. **11**, 643-652 DOI: 10.1007/s10404-011-0830-5.
68. Delgado, S.M.T., D.J. Kinahan, L.A.N. Julius, A. Mallette, D.S. Ardila, R. Mishra, C.M. Miyazaki, J.G. Korvink, J. Ducrée, and D. Mager *Wirelessly powered and remotely controlled valve-array for highly multiplexed analytical assay automation on a centrifugal microfluidic platform*. Biosensors & Bioelectronics, 2018. **109**, 214-223 DOI: 10.1016/j.bios.2018.03.012.
69. Haeberle, S., N. Schmitt, R. Zengerle, and J. Ducrée *Centrifugo-magnetic pump for gas-to-liquid sampling*. Sensors and Actuators A-Physical, 2007. **135**, 28-33 DOI: 10.1016/j.sna.2006.09.001.
70. Kim, J., S. Hee Jang, G. Jia, J.V. Zoval, N.A. Da Silva, and M.J. Madou *Cell lysis on a microfluidic CD (compact disc)*. Lab on a Chip, 2004. **4**, 516-22 DOI: 10.1039/b401106f.
71. Burger, R., D. Kirby, M. Glynn, C. Nwankire, M. O'Sullivan, J. Siegrist, D. Kinahan, G. Aguirre, G. Kijanka, R.A. Gorkin, 3rd, and J. Ducree *Centrifugal microfluidics for cell analysis*. Current Opinion in Chemical Biology, 2012. **16**, 409-14 DOI: 10.1016/j.cbpa.2012.06.002.
72. Smith, S., R. Sewart, H. Becker, P. Roux, and K. Land *Blister pouches for effective reagent storage on microfluidic chips for blood cell counting*. Microfluidics and Nanofluidics, 2016. **20**, DOI: 10.1007/s10404-016-1830-2.
73. Krauss, S.T., M.S. Woolf, K.C. Hadley, N.M. Collins, A.Q. Nauman, and J.P. Landers *Centrifugal microfluidic devices using low-volume reagent storage and inward fluid displacement for presumptive drug detection*. Sensors and Actuators B: Chemical, 2019. **284**, 704-710 DOI: 10.1016/j.snb.2018.12.113.
74. Czurratis, D., Y. Beyl, S. Zinober, F. Larmer, and R. Zengerle *A novel concept for long-term pre-storage and release of liquids for pressure-driven lab-on-a-chip devices*. Journal of Micromechanics and Microengineering, 2015. **25**, DOI: 10.1088/0960-1317/25/4/045002.
75. Mishra, R., R. Alam, D. McAuley, T. Bharaj, D. Chung, D.J. Kinahan, C. Nwankire, K.S. Anderson, and J. Ducrée *Centrifugal automation of highly customisable, bead-based immunoassays using solvent-selective routing*. Scientific Reports, 2021.
76. Strohmeier, O., M. Keller, F. Schwemmer, S. Zehnle, D. Mark, F. von Stetten, R. Zengerle, and N. Paust *Centrifugal microfluidic platforms: advanced unit operations and applications*. Chemical Society Reviews, 2015. **44**, 6187-6229 DOI: 10.1039/c4cs00371c.
77. Mark, D., P. Weber, S. Lutz, M. Focke, R. Zengerle, and F. von Stetten *Aliquoting on the centrifugal microfluidic platform based on centrifugo-pneumatic valves*. Microfluidics and Nanofluidics, 2011. **10**, 1279-1288 DOI: 10.1007/s10404-010-0759-0.
78. Kinahan, D.J., R. Burger, A. Vembadi, N.A. Kilcawley, D. Lawlor, M.T. Glynn, and J. Ducrée, *Baking-Powder Driven Centripetal Pumping Controlled by Event-*

Triggering of Functional Liquids, in *2015 28th IEEE International Conference on Micro Electro Mechanical Systems (MEMS 2015)*. 2015: Estoril, Portugal. p. 504-507 DOI: 10.1109/MEMSYS.2015.7051002.

79. Schwemmer, F., S. Zehnle, D. Mark, F. von Stetten, R. Zengerle, and N. Paust *A microfluidic timer for timed valving and pumping in centrifugal microfluidics*. Lab on a Chip, 2015. **15**, 1545-1553 DOI: 10.1039/C4LC01269K.
80. Deyn, L.H.v. and J. Ducrée, *The centrifugo-pneumatic Lab-on-a-Disk platform: Towards robust flow control for larger-scale functional integration*, in *23rd International Conference on Miniaturized Systems for Chemistry and Life Sciences (μTAS 2019)*, A.H. Petra Dittrich, and Emanuel Delamarche, Editor., The Chemical and Biological Microsystems Society (CBMS): Basel, Switzerland. p. 922–923
81. Nwankire, C.E., D.S. Chan, J. Gaughran, R. Burger, R. Gorkin, 3rd, and J. Ducrée *Fluidic automation of nitrate and nitrite bioassays in whole blood by dissolvable-film based centrifugo-pneumatic actuation*. Sensors, 2013. **13**, 11336-49 DOI: 10.3390/s130911336.
82. Mishra, R., G. Reilly, M. Agnew, A. Garvey, C. Rogers, E. Andrade, H. Ma, S. Fitzgerald, J. Zapatero, R. O'Kennedy, and J. Ducrée, *Laser-Actuated Centrifugo-Pneumatic Flow Control Towards 'Sample-to-Answer' Integrated Detection of Multi-Marker Panels at the Point-of-Care*, in *2018 IEEE Micro Electro Mechanical Systems (MEMS)*. 2018: Belfast, Northern Ireland. p. 1185-1188 DOI: 10.1109/MEMSYS.2018.8346774.
83. Godino, N., E. Comaskey, R. Gorkin, and J. Ducrée, *Centrifugally Enhanced Paper Microfluidics*, in *2012 IEEE 25th International Conference on Micro Electro Mechanical Systems (MEMS)*. 2012: Paris, France DOI: 10.1109/MEMSYS.2012.6170352.
84. Soroori, S., L. Kulinsky, H. Kido, and M. Madou *Design and implementation of fluidic micro-pulleys for flow control on centrifugal microfluidic platforms*. Microfluidics and Nanofluidics, 2014. **16**, 1117-1129 DOI: 10.1007/s10404-013-1277-7.
85. van Heeren, H. *Standards for connecting microfluidic devices?* Lab on a Chip, 2012. **12**, 1022-1025 DOI: 10.1039/C2LC20937C.
86. Stavis, S.M. *A glowing future for lab on a chip testing standards*. Lab on a Chip, 2012. **12**, 3008-11 DOI: 10.1039/c2lc40511c.
87. Reyes, D.R., H.v. Heeren, S. Guha, L.H. Herbertson, A.P. Tzannis, J. Ducrée, H. Bissig, and H. Becker *Accelerating Innovation and Commercialization Through Standardization of Microfluidic-Based Medical Devices*. Lab on a Chip, 2021. DOI: 10.1039/D0LC00963F.
88. Ducrée, J., M. Gravitt, R. Walshe, M. Etzrodt, and T. Harrington, *Open Platform for Blockchain-Enabled Crowdsourcing of Value and Supply Chains Exemplified by Lab-on-a-Disc*.
89. Ducrée, J., *An open-platform approach for promoting democratisation of value creation in RTD enabled by distributed ledger technologies*, in *steps BCN -*

#CRYPTSCIENCE19 #SPONBC19, M.E.a.S. Bartling, Editor. 2019, Blockchain for Science GmbH: Barcelona, Catalunya, Spain

90. Ducrée, J., M. Etzrodt, B. Gordijn, M. Gravitt, S. Bartling, R. Walshe, and T. Harrington *Blockchain for Organising Effective Grass-Roots Actions on a Global Commons: Saving The Planet*. Frontiers in Blockchain, 2020. **3**, 33 DOI: 10.3389/fbloc.2020.00033.
91. Ducrée, J., M. Etzrodt, S. Bartling, R. Walshe, T. Harrington, N. Wittek, S. Posth, K.W.A. Ionita, W. Prinz, D. Kogias, T. Paixão, I. Peterfi, and J. Lawton *Unchaining collective intelligence for science, research and technology development by blockchain-boosted community participation*. Frontiers in Blockchain, 2021. DOI: 10.3389/fbloc.2021.631648.
92. Ducrée, J. *Research - A blockchain of knowledge?* Blockchain - Research and Applications, 2020. **1**, 100005 DOI: 10.1016/j.bcra.2020.100005.
93. Ducrée, J. *Efficient Development of Integrated Lab-On-A-Chip Systems Featuring Operational Robustness and Manufacturability*. Micromachines, 2019. **10**, DOI: 10.3390/mi10120886.